Tectonophysics 719–720 (2017) 66–85

Contents lists available at ScienceDirect

Tectonophysics

journal homepage: www.elsevier.com/locate/tecto

Stratigraphic record of Pliocene-Pleistocene basin evolution and deformation within the Southern San Andreas Fault Zone, Mecca Hills, California

James C. McNabb [a,*], Rebecca J. Dorsey [a], Bernard A. Housen [b], Cassidy W. Dimitroff [b], Graham T. Messé [b]

[a] Department of Earth Sciences, 1272 University of Oregon, Eugene, OR 97403-1272, USA
[b] Department of Geology, 516 High Street, Western Washington University, Bellingham, WA 98225-9080, USA

ARTICLE INFO

Article history:
Received 30 July 2016
Received in revised form 28 February 2017
Accepted 24 March 2017
Available online 28 March 2017

Keywords:
San Andreas fault
Mecca Hills
Gulf of California
Strike-slip basins
Magnetostratigraphy
Tectonostratigraphy

ABSTRACT

A thick section of Pliocene-Pleistocene nonmarine sedimentary rocks exposed in the Mecca Hills, California, provides a record of fault-zone evolution along the Coachella Valley segment of the San Andreas fault (SAF). Geologic mapping, measured sections, detailed sedimentology, and paleomagnetic data document a 3–5 Myr history of deformation and sedimentation in this area. SW-side down offset on the Painted Canyon fault (PCF) starting ~3.7 Ma resulted in deposition of the Mecca Conglomerate southwest of the fault. The lower member of the Palm Spring Formation accumulated across the PCF from ~3.0 to 2.6 Ma during regional subsidence. SW-side up slip on the PCF and related transpressive deformation from ~2.6 to 2.3 Ma created a time-transgressive angular unconformity between the lower and upper members of the Palm Spring Formation. The upper member accumulated in discrete fault-bounded depocenters until initiation of modern deformation, uplift, and basin inversion starting at ~0.7 Ma.

Some spatially restricted deposits can be attributed to the evolution of fault-zone geometric complexities. However, the deformation events at ca. 2.6 Ma and 0.7 Ma are recorded regionally along ~80 km of the SAF through Coachella Valley, covering an area much larger than mapped fault-zone irregularities, and thus require regional explanations. We therefore conclude that late Cenozoic deformation and sedimentation along the SAF in Coachella Valley has been controlled by a combination of regional tectonic drivers and local deformation due to dextral slip through fault-zone complexities. We further propose a kinematic link between the ~2.6–2.3 Ma angular unconformity and a previously documented but poorly dated reorganization of plate-boundary faults in the northern Gulf of California at ~3.3–2.0 Ma. This analysis highlights the potential for high-precision chronologies in deformed terrestrial deposits to provide improved understanding of local- to regional-scale structural controls on basin formation and deformation along an active transform margin.

1. Introduction

The formation and deformation of sedimentary basins is widely documented along continental transform faults (Crowell, 1974; Christie-Blick and Biddle, 1985; Sadler et al., 1993; Weldon et al., 1993; Aksu, 2000; Seeber et al., 2006, 2010), yet the controls on strike-slip basin evolution remain incompletely understood. Models that predict transpression and transtension due to relative plate-motion obliquity along strike-slip faults fail to describe observed patterns of uplift and subsidence along the San Andreas fault (SAF) (e.g., Spotila et al., 2007a, b), suggesting the influence of additional factors such as structural complexity, rock strength, crustal anisotropy, or changes in local and regional (plate boundary-scale) kinematics. Sedimentary rocks deposited and subsequently uplifted along strike-slip faults record the basinal response to fault-zone processes, offering unique insights into the 4-D evolution of strain in these settings.

The Mecca Hills on the northeast side of Coachella Valley, southern California, superbly expose a >1.3 km-thick section of Pliocene-Pleistocene terrestrial sedimentary rocks along the southern San Andreas fault and associated strike-slip faults. Recent uplift and erosion in the Mecca Hills allow for detailed sedimentological and stratigraphic analysis, making it an excellent natural laboratory to study the stratigraphic record of deformation along strike-slip faults. Previous workers have documented the stratigraphy and modern structure of the Mecca Hills (summarized below), but until this study the evolution and chronology of depositional systems in response to fault-zone evolution through time have not been fully understood. We combine geologic mapping, stratigraphic analysis, magnetostratigraphic data, and determination

* Corresponding author at: ExxonMobil, Exploration Company, 22777 Springwoods Village Parkway, 77389 Spring, TX, USA.
E-mail address: james.c.mcnabb@exxonmobil.com (J.C. McNabb).

http://dx.doi.org/10.1016/j.tecto.2017.03.021
0040-1951/

of sedimentary provenance to reconstruct past landscapes and environments in response to crustal deformation. This allows us to interpret a 3–4 Myr history of basin formation and deformation in the Mecca Hills, and assess the underlying controls on vertical crustal motions along this section of the southern SAF zone.

2. Geologic setting and prior work

2.1. Southern San Andreas Fault Zone

The southern SAF zone (Fig. 1) has been the locus of relative plate motion between the Pacific and North American plates since its inception in the Coachella Valley between ca. 6 and 12 Ma (e.g., Atwater, 1970; Stock and Hodges, 1989; Ingersoll and Rumelhart, 1999; Oskin and Stock, 2003a, b; Dorsey et al., 2011). The Coachella Valley segment of the SAF consists of a main strand that bounds the northeast Coachella Valley and Salton Trough, and terminates in the southeast Salton Sea at the Brawley seismic-zone releasing step-over (Fig. 1). Northwest of the study area, the southern SAF zone splits into the Banning and Mission Creek faults near a major restraining step-over in San Gorgonio Pass (Fig. 1).

Late Cenozoic oblique transform tectonics has produced large-scale transtensional and transpressional features within the southern SAF system since late Miocene time. Regional transtension was partitioned into extension on the low-angle west Salton detachment fault and strike-slip offset on the SAF from latest Miocene to early Pleistocene time (e.g., Axen and Fletcher, 1998; Dorsey et al., 2011). At ~1.3 to 1.1 Ma a major tectonic reorganization resulted in initiation of the San Jacinto fault zone and termination of the West Salton detachment fault (e.g. Morton and Matti, 1993; Lutz et al., 2006; Janecke et al., 2010; Dorsey et al., 2012; Fattaruso et al., 2016), which transferred a significant but uncertain fraction of relative plate motion from the southern SAF to the San Jacinto fault zone (Fig. 1).

The modern Salton Trough and Coachella Valley basin fill consists of a sediment wedge that onlaps basement rocks of the Santa Rosa Mountains in the southwest, and thickens northeastward to 4–5 km against the SAF (Langenheim et al., 2005; Dorsey and Langenheim, 2015). Strong oblique extension and possible lithospheric rupture beneath the Salton Trough appears to have deflected the Moho to shallower depths leading to the ongoing creation of young metasedimentary rocks (Fuis et al., 1984; Elders and Sass, 1988; Parsons and McCarthy, 1996; Dorsey, 2010; Lekic et al., 2011). In contrast, transpression and crustal shortening northwest of the Coachella Valley at the San Gorgonio Pass restraining step-over has thrust Mesozoic and Cenozoic basement rocks over young basin sediments (Matti and Morton, 1993; Dibblee, 1997; Yule and Sieh, 2003; Langenheim et al., 2005). Recent studies document northeast tilting of the crustal-scale block between the SAF and San Jacinto fault over the past ~1.2 Ma, which likely is caused by crustal loading from highly oblique transpression along the SAF in Coachella Valley (Fattaruso et al., 2014; Dorsey and Langenheim, 2015).

Discrete elongate zones of fault-bounded uplift along the southern SAF in the Indio Hills, Mecca Hills, and Durmid Hill define the northeast boundary of Coachella Valley and Salton Trough (Fig. 1). Between areas of uplift, the geomorphic expression of the SAF varies from expressionless in lowland areas to vegetation lineaments, dextrally offset geomorphic features, fault sags, and scarps (e.g. Sylvester and Smith, 1976; Keller et al., 1982; Sieh and Williams, 1990; Dibblee, 1997; Behr et al., 2010; Gray et al., 2014). Recent studies of InSAR and GPS data (Lindsey and Fialko, 2013), seismic hypocenter relocation (Lin et al.,

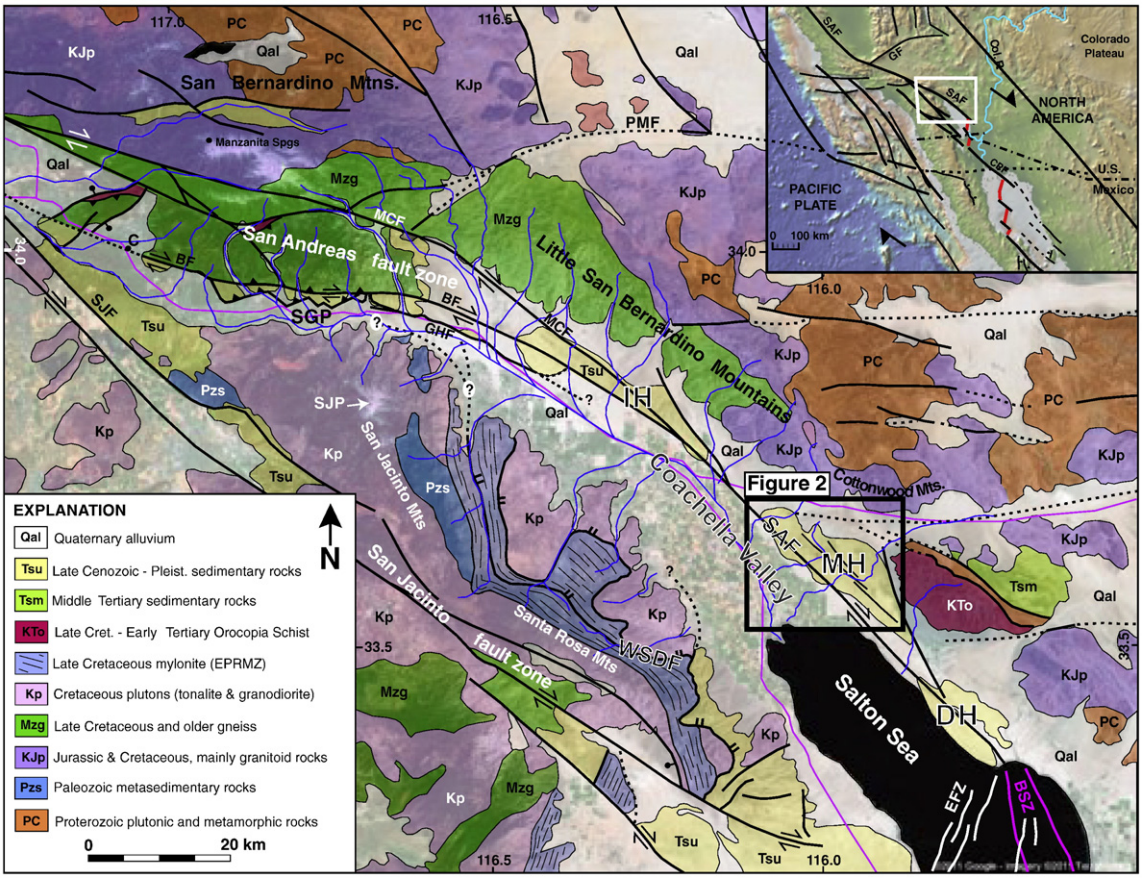

Fig. 1. Geologic map of the Coachella Valley. Modified from Dorsey and Langenheim (2015). Abbreviations: BF, Banning fault; BSZ, Brawley seismic zone; DH, Durmid Hill; EFZ, Extra fault zone; IH, Indio Hills; MCF, Mission Creek fault; MH, Mecca Hills; PMF, Pinto Mtn. fault; SAF, San Andreas fault; SGP, San Gorgonio Pass; SJF, San Jacinto fault; SJP, San Jacinto Peak; WSDF, West Salton detachment fault.

2007; Fuis et al., 2012), and kinematic finite-element fault modeling (Fattaruso et al., 2014, Fattaruso et al., 2016) suggest a 60°–70° northeast dip for the Coachella Valley segment of the SAF, previously assumed to be sub-vertical. Fattaruso et al. (2014) concluded that modeling a NE-dipping SAF through Coachella Valley better aligns seismic hypocenters with the fault at depth, and generates patterns of deformation that closely match modern subsidence and uplift.

2.2. Mecca Hills

The Mecca Hills are located on the northeast side of the Coachella Valley segment of the SAF, about 10 km north of the Salton Sea (Fig. 1). They define an elongate zone of heterogeneous strike-slip-related deformation and uplift of upper Cenozoic terrestrial strata cut by high-angle sub-parallel faults and broad to tight en-echelon folds (Fig. 2; Sylvester and Smith, 1976; Boley et al., 1994; Sheridan and Weldon, 1994; Dibblee, 1997; Sylvester, 1999). Previous workers proposed various models for transpressive deformation in the Mecca Hills. Sylvester and Smith (1976) concluded that upward diverging and flattening oblique reverse faults, or 'flower' structures, are the dominant structural style in the Mecca Hills, with passive deformation of the sedimentary cover occurring above highly strained basement rock. Sheridan and Weldon (1994) noted the importance of inward verging reverse faults and folds, or 'pooch' structures, formed by propagation of reverse faults on the limbs of growing anticlines and rooted in weak sedimentary units. Smaller-scale transtensional horsetail splay faults accompany some of the larger faults in the Mecca Hills, a feature typical of wrench-style tectonics (Fig. 2; Wilcox et al., 1973; Sylvester and Smith, 1976; Sheridan and Weldon, 1994; Miller, 1998).

Sedimentary strata >1300 m thick in the Mecca Hills includes the Mecca Conglomerate, Palm Spring Formation, and Ocotillo Conglomerate (Figs. 2, 3), which were first described and named by Dibblee (1954). The main exposures of Mecca Conglomerate in the central Mecca Hills are limited to the SW side of the Painted Canyon fault (PCF), where it rests nonconformably on crystalline basement rock and is conformably overlain by the Palm Spring Formation in lower Painted Canyon (Figs. 3, 4; McNabb, 2013). Previous workers suggested that coarse deposits exposed along the Grotto and Hidden Spring faults in the southeast Mecca Hills (Fig. 2) are equivalent to the Mecca Formation (Boley et al., 1994), but abrupt lateral facies changes and spatially restricted deposits commonly preclude confident time-stratigraphic correlations. The lower member of the Palm Spring Formation consists of fluvial interbedded sandstone and siltstone; a prominent angular unconformity between the lower and upper members records an important phase of intra-basinal deformation and erosion within the fault zone (Figs. 3, 4). The PCF appears to control the distribution of deposits and exposures of basement rock in the central to northwestern Mecca Hills (Figs. 4, 5).

Sylvester and Smith (1976) divided the central Mecca Hills into three structural blocks bounded by the SAF and PCF: (1) the basin block southwest of the SAF; (2) central block between the SAF and PCF, and (3) the platform block northeast of the PCF (Figs. 2, 4). Each block contains a distinct stratigraphy and style of deformation. The basin block is deformed in a narrow belt of uplifted and eroding deposits

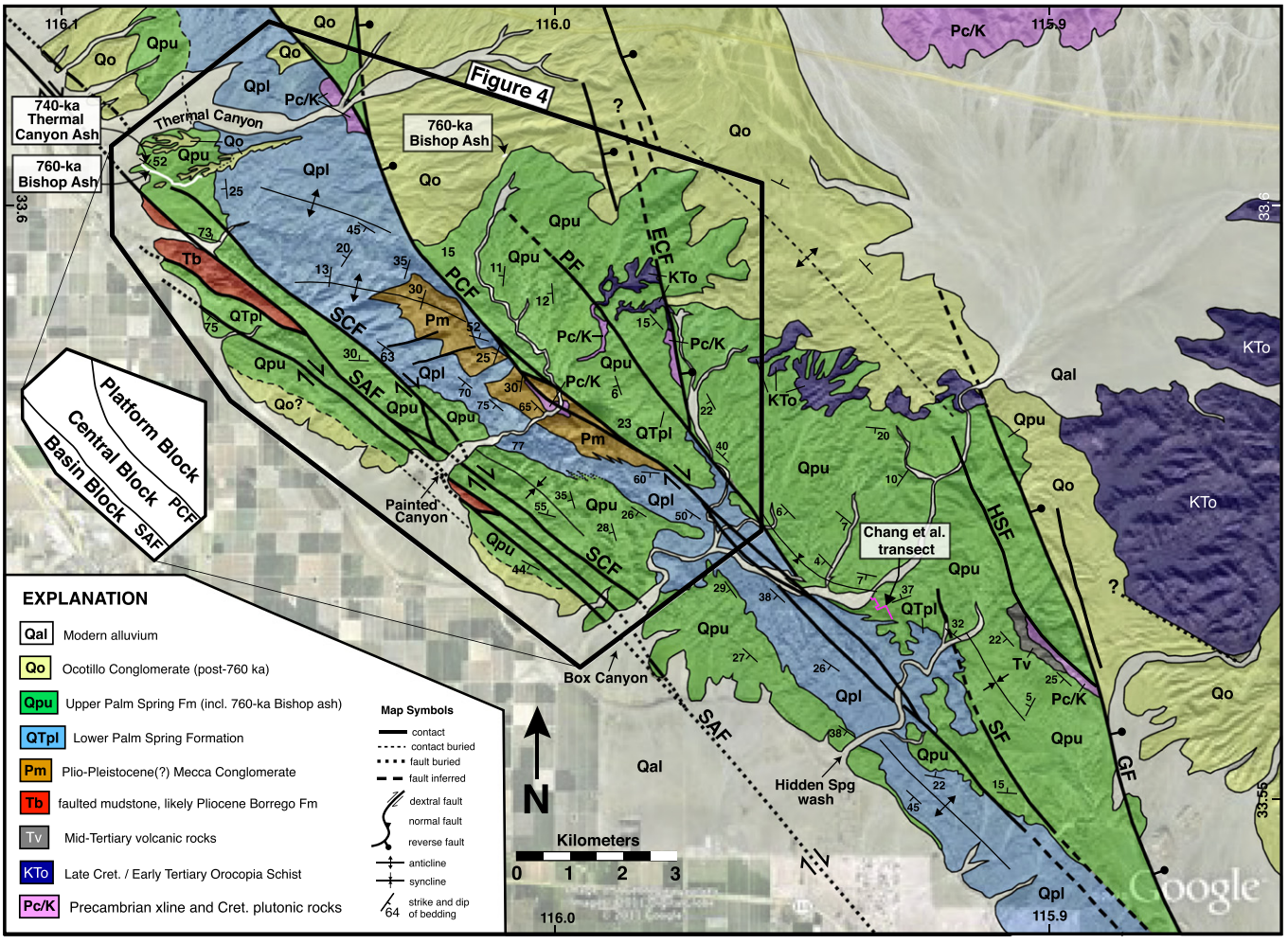

Fig. 2. Geologic map of the Mecca Hills, compiled from Sylvester and Smith (1976), Rymer (1991, 1994), Weldon (2011, personal commun.), and McNabb (2013). Location shown in Fig. 1. Abbreviations: SAF, San Andreas fault; SCF, Skeleton Canyon Fault; PCF, Painted Canyon fault; PF, Platform Fault; ECF, Eagle Canyon fault; HSF, Hidden Spring Fault; GF, Grotto Fault.

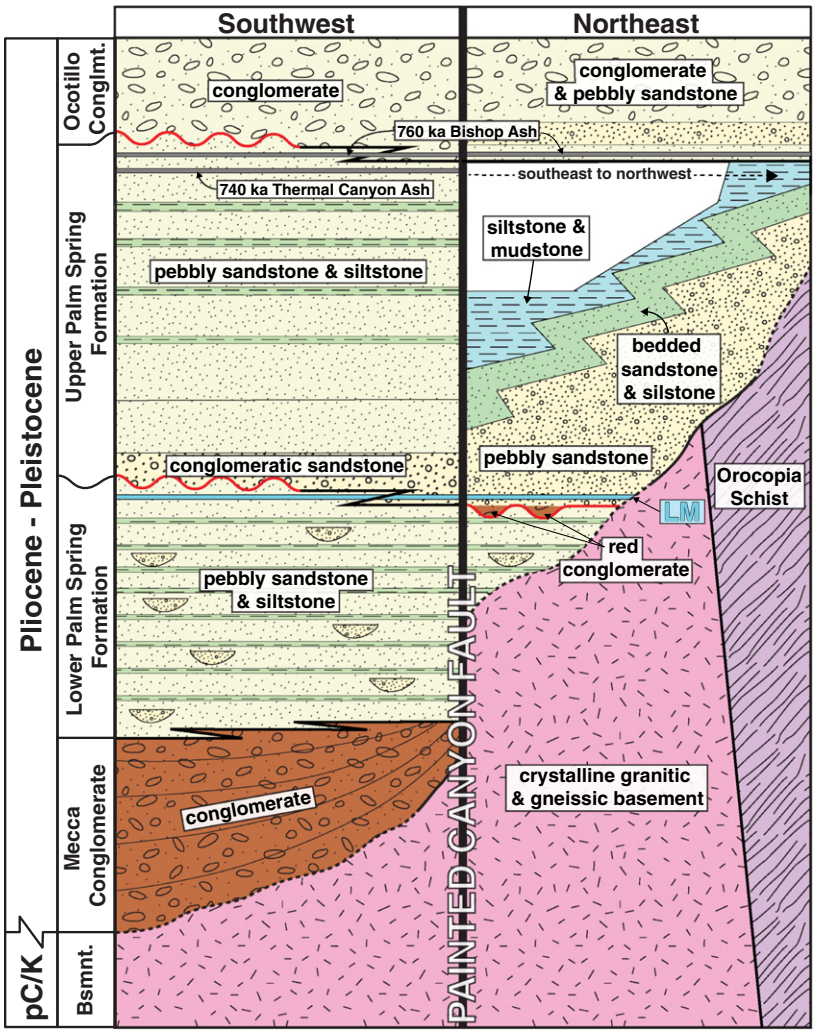

Fig. 3. Simplified diagram of stratigraphic and basement relationships southwest and northeast of the Painted Canyon fault near Painted Canyon.

along the SW side of the SAF, and is otherwise mostly subsiding and buried beneath modern alluvium of the Coachella Valley. The central block contains the thickest exposed section of sedimentary strata in the Mecca Hills, and is an area of intense transpressional deformation. The platform block consists of shallow basement rock with overlying mostly undeformed shallowly dipping (<15°) sedimentary strata (Figs. 2, 3).

Previous attempts to date deposits in the Mecca Hills were based on the presence of the 0.76-Ma Bishop Ash high in the section and the predominantly reversed magnetic polarity of the section that is thought to represent the Matuyama magnetochron (2.58- to 0.78-Ma; Chang et al., 1987; Boley et al., 1994). These constraints were used to conclude that much of the upper member of the Palm Spring Formation exposed in the Mecca Hills was deposited between 2.58 and 0.76 Ma (Chang et al., 1987; Boley et al., 1994). Boley (1993) and Boley et al. (1994) documented strong normal-polarity overprinting in many of their paleomagnetic samples in the Mecca and Indio Hills, and suggested that post-0.78 Ma magnetic overprinting may affect much of the Palm Spring Formation. They found step-wise thermal demagnetization to be more effective at removing magnetic overprints in their samples than alternating-field demagnetization. Chang et al. (1987) successfully documented 4 magnetic reversals and 5 magnetochrons in the upper member of the Palm Spring Formation, which they assigned to the reversed-polarity Matuyama magnetochron and the normal-polarity Jaramillo (1.07–0.99 Ma) and Olduvai (1.94–1.79 Ma) subchrons.

3. Methods

3.1. Geologic mapping and field methods

Detailed geologic mapping of the central Mecca Hills was conducted over the course of three field seasons between 2012 and 2014 (McNabb, 2013). Stratigraphic formations, sedimentary lithofacies, and geologic contacts were mapped on high-resolution satellite imagery with UTM grid overlay at 1:10,000 scale. Bedrock exposures permit some contacts to be inferred from satellite imagery, which proved useful for mapping inaccessible high-relief areas.

Stratigraphic sections were measured in the field with a 1.5-m Jacob's staff at the meter to sub-meter scale, accompanied by detailed facies descriptions. Section 1 is a composite of 5 sections measured northeast of the PCF (Fig. 4) that were correlated using distinctive marker horizons. Due to low bedding dips, section 1 spans a long distance and crosses significant lateral facies changes. In order to constrain facies architecture along this composite path, several short intervals within section 1 were measured with photography in vertical cliff exposures where direct measurements were unattainable. This technique allowed us to correlate lateral facies changes that are visible high in the canyon walls from SE to NW. Section 3 was measured in lower Painted Canyon perpendicular to the strike of bedding (Figs. 4, 6B).

Determination of paleocurrent directions was conducted by measuring (1) the strike and dip of imbricated clasts in conglomeratic beds, (2)

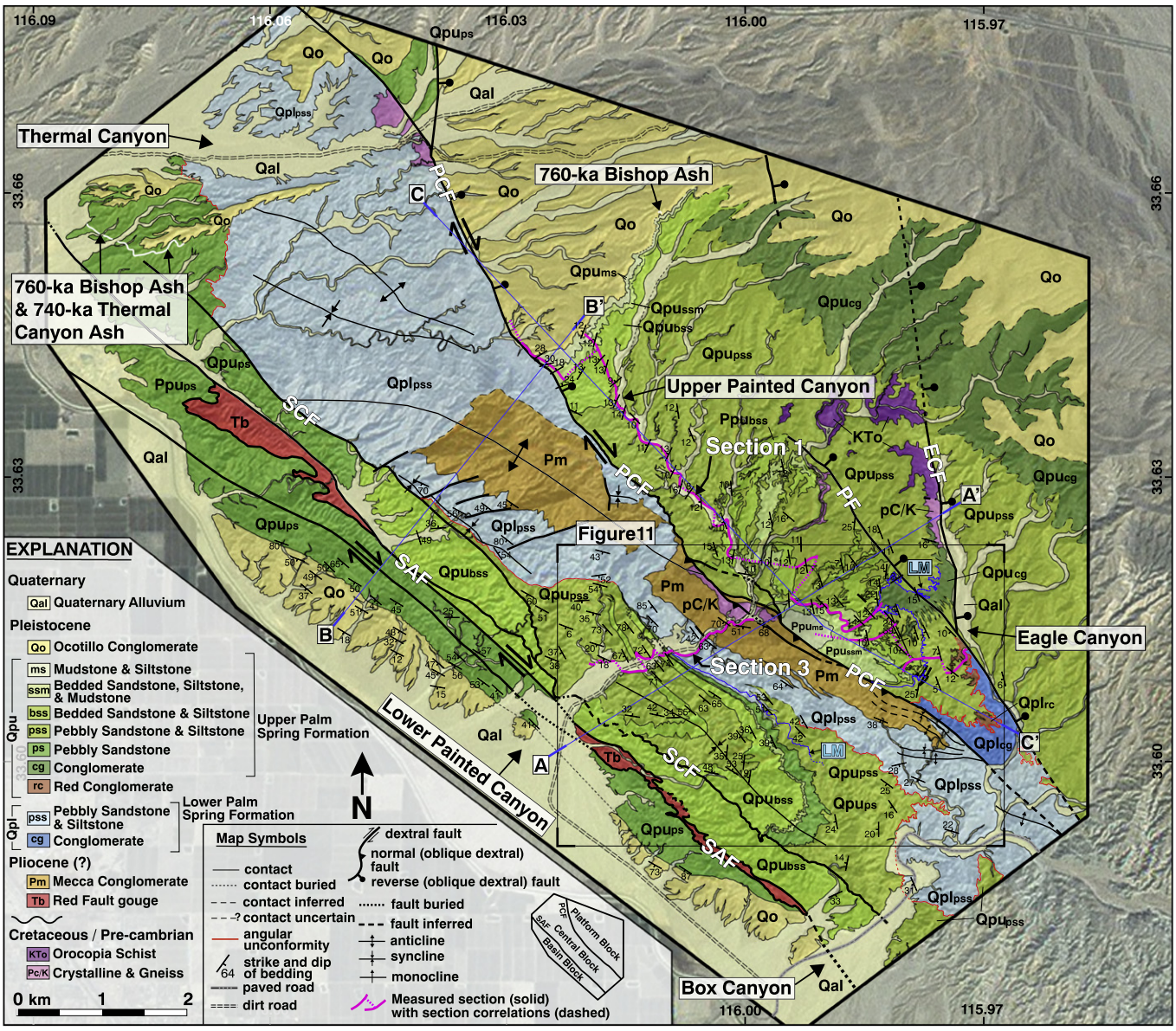

Fig. 4. Geologic map of the Mecca Hills near Painted Canyon (this study). Abbreviations: SAF, San Andreas fault; SCF, Skeleton Canyon fault; PCF, Painted Canyon fault; PF, Platform fault; ECF, Eagle Canyon fault.

strike and dip of cross-bed foresets, (3) trend and plunge of current lineations and tool marks on the base of beds, and (4) trend and plunge of fluvial channel axes. Imbricated clast and cross-bed foreset measurements provide unique paleoflow directions, while current lineations, tool marks, and fluvial channel axes must be coupled with other data to determine a unique paleoflow direction.

Conglomerate clast counts were conducted by establishing a ~1 m square on rock outcrops, randomly selecting at least 100 clasts using a systematic grid system, and tallying relative abundances of various compositions. The most distinctive composition is Orocopia Schist sourced from local basement and the Orocopia Mountains southeast of the Mecca Hills (e.g., Jacobson et al., 2007). Other compositions of Precambrian to Cretaceous tonalite and gneiss and Tertiary volcanic rocks are sourced from local basement and the Cottonwood Mountains (Fig. 1).

3.2. Paleomagnetic analysis

We incorporate recently acquired magnetostratigraphic data (Messé, 2014; Dimitroff, 2015) sampled in conjunction with this study for sections 1 and 3. The challenges raised by prior paleomagnetic studies in the Mecca Hills allowed us to tailor our methods of sample collection and analysis to specifically address these issues. Samples were collected in the field using three methods: (1) handheld gasoline powered drill to sample 1-inch diameter oriented cores; (2) collection of oriented block samples that were later drilled in the lab; and (3) 1-inch diameter by 1-inch deep plastic collection cylinders to collect poorly indurated sediments. Sampling of section 3 yielded 57 drilled core sites and 1 oriented hand sample site, with an average stratigraphic spacing of ~22 m between sample sites. Due to the restricted (wilderness area) access for the gasoline-powered drill in section 1, these samples consist of 40 oriented hand sample sites and 7 plastic-cylinder-sample sites with an average stratigraphic spacing of ~11 m between sites. The number of samples varied between sites based on sampling technique and rock quality. On average we collected 4–6 cores at drill sites, 1–5 blocks at oriented-block sites, and 5–7 plastic tubes at soft-sediment sites.

Samples were analyzed at Western Washington University (WWU), using alternating-field and thermal demagnetization techniques to

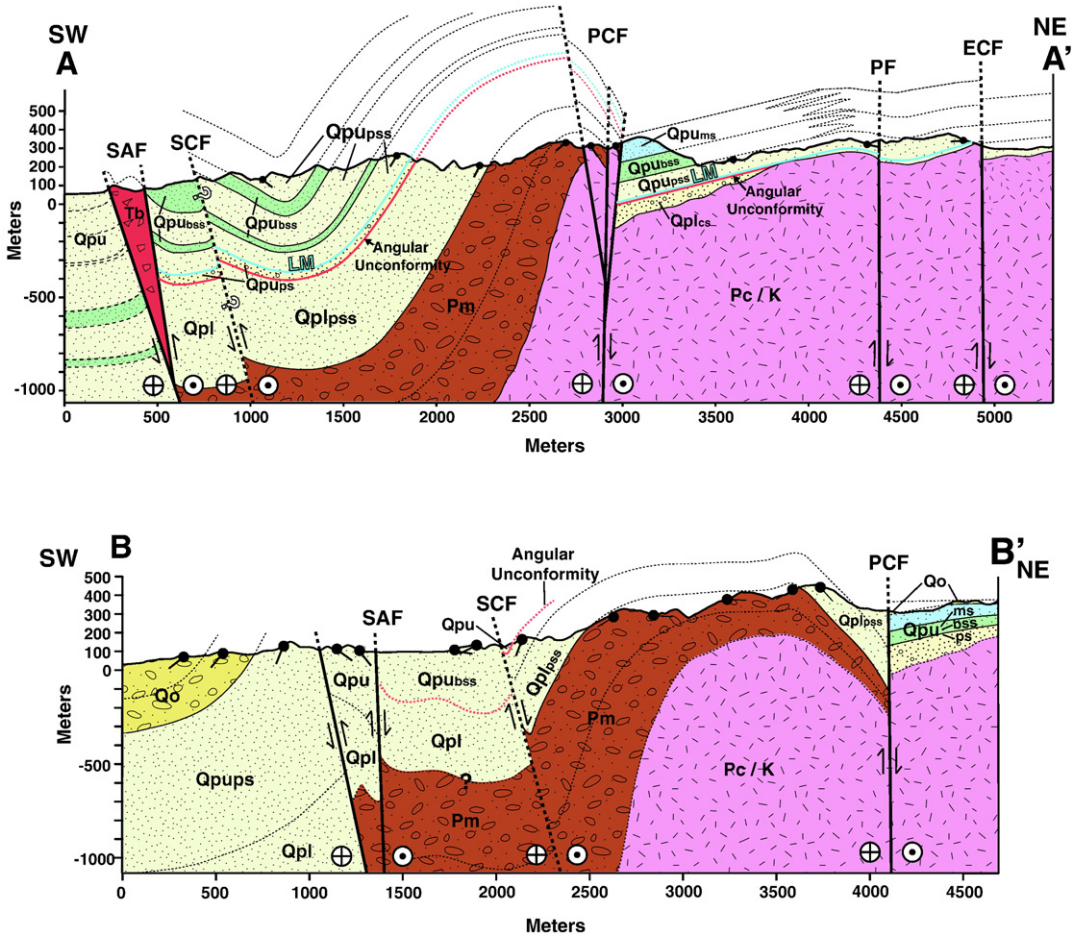

Fig. 5. Geologic cross section from lines A–A′ and B–B′ in Fig. 4. Abbreviations: SAF, San Andreas fault; SCF, Skeleton Canyon Fault; PCF, Painted Canyon fault; PF, Platform fault; ECF, Eagle Canyon fault.

determine the characteristic remanence of the samples and the original magnetic polarity of the deposits. All samples were measured with a 2-G cryogenic magnetometer in a magnetically shielded room in the WWU lab. The plastic-tube samples cannot be thermally demagnetized, and alternating-field demagnetization often is ineffective at removing magnetic overprints. In this study, we included results from plastic cylinders only in selected cases where the results were well defined. For some other sites, all samples were destroyed during transport, processing, or measurement - these are noted in Table DR-1. The paleomagnetic data, coupled with presence of the 0.76-Ma Bishop Ash correlated into the upper part of section 1 (Fig. 6A), were used to estimate sediment accumulation rates and ages for sedimentary strata in the central Mecca Hills.

4. Results

4.1. Geologic map and cross sections

The geologic map (Fig. 4) and cross sections (Fig. 5) provide important context for analysis and interpretation of sedimentary rocks in this study (McNabb, 2013). Sedimentary strata in the central Mecca Hills nonconformably overlie Precambrian and Cretaceous basement in a > 1300-m thick succession that records late Cenozoic terrestrial sedimentation over the past 4–5 Myr. Previous workers noted the diversity of facies and abrupt lateral and vertical facies changes in the Mecca Hills, especially in relation to structures (e.g., Sylvester and Smith, 1976; Chang et al., 1987; Boley et al., 1994; Sheridan and Weldon, 1994; McNabb, 2013). Our mapping confirms and documents the contrast between the diverse localized facies of the upper member of the Palm Spring Formation, and the widespread relatively uniform facies distribution of the lower member of the Palm Spring Formation in the central Mecca Hills (Fig. 4), similar to the findings of previous workers in the southeast Mecca Hills. Our geologic cross sections (Fig. 5) refine the distribution of sedimentary sequences, basement relationships, and structural styles of the platform, central, and basin blocks. Measured stratigraphic sections are presented in Fig. 6.

4.2. Sedimentary lithofacies

4.2.1. Mecca Conglomerate (Pm)

The Mecca Conglomerate, which rests nonconformably on basement in lower Painted Canyon (Figs. 3, 4), has a measured thickness of 330 m (Fig. 6B). The lower ~150 m consist of poorly sorted, weakly bedded (~5–10 m thick), interbedded pebble-cobble to small-boulder conglomerate and pebbly sandstone with dominantly gneissic clasts and lesser granitic and Orocopia Schist clasts derived from nearby basement (Table 1, Figs. 6B, 7A). The upper ~180 m consists of mostly pebble to cobble conglomerate with better defined beds ranging from ~1 to 5 m thick. Imbricated clasts indicate overall SE- to NW-directed paleoflow (Fig. 6B). The upper part of Mecca Conglomerate in lower Painted Canyon is interbedded with and gradationally fines up-section into the overlying lower member of the Palm Spring Formation (Fig. 6B).

We conclude that the lower part of the Mecca Conglomerate was deposited by debris flows in proximal alluvial fans based on the abundance of poorly sorted, weakly bedded conglomerate (e.g., Blair, 1987a), and the overall semi-radial pattern of paleocurrent directions (Fig. 6B) that suggest transport emanating from a point source (i.e. canyon at a topographic range front). Locally derived clast compositions

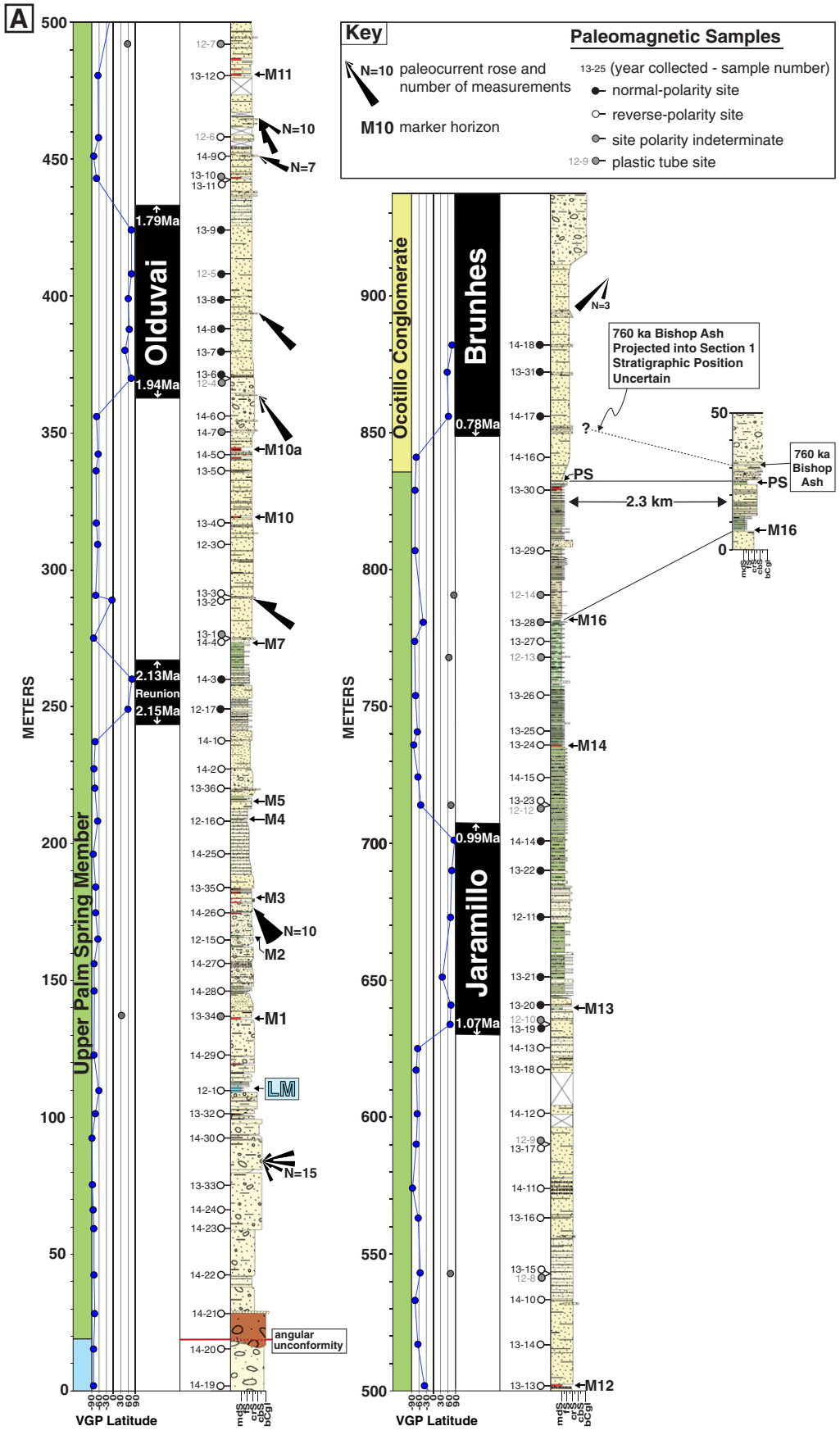

Fig. 6. A. Measured stratigraphic section 1, northeast of the Painted Canyon fault with paleomagnetic site VGP latitudes and our preferred correlations to the Geomagnetic Polarity Time Scale (GPTS). B. Measured stratigraphic section 3, southwest of the Painted Canyon fault with paleomagnetic site VGP latitudes.

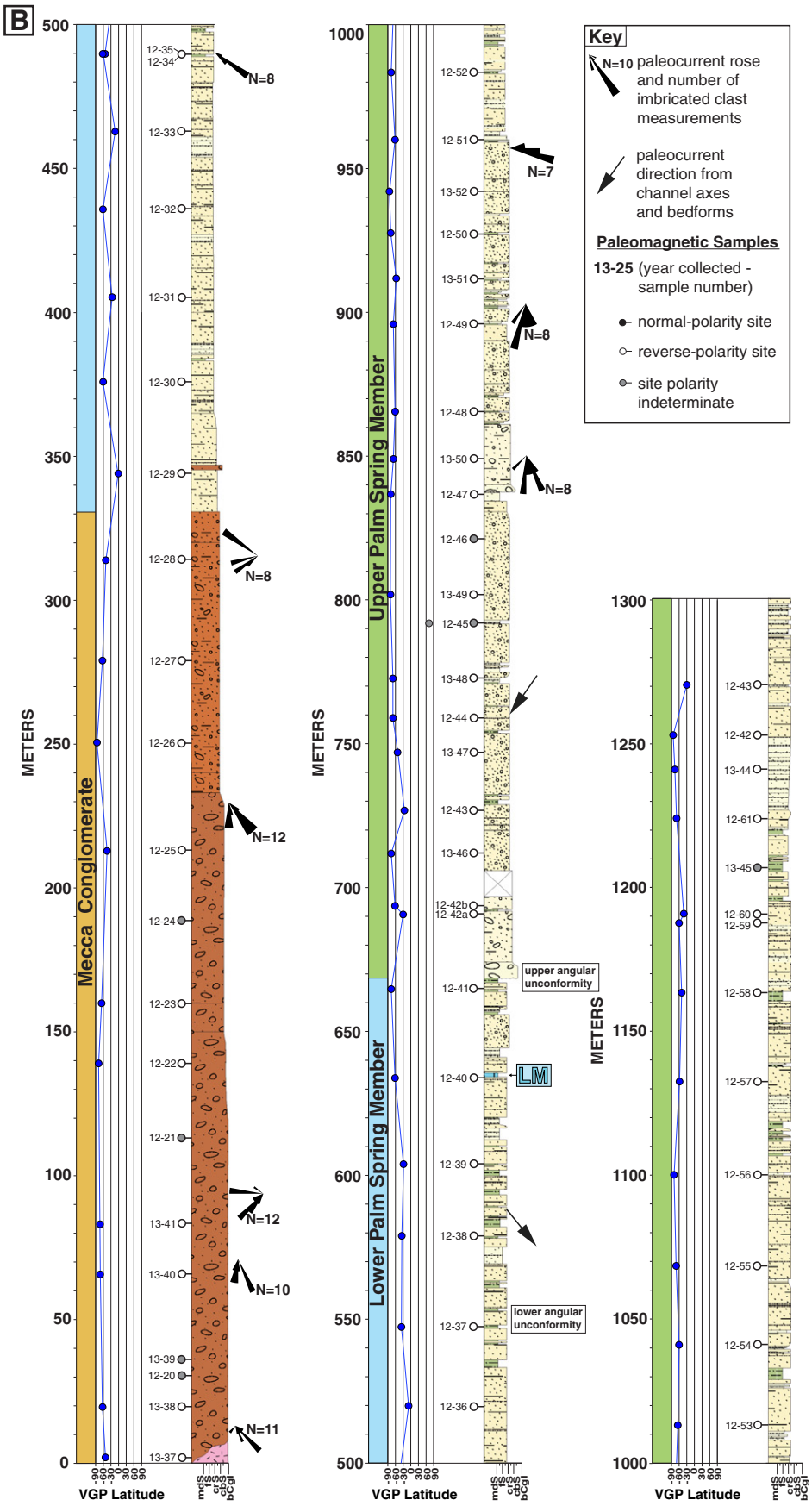

Fig. 6 (*continued*).

Table 1
Descriptions and interpretations of sedimentary lithofacies in the study area.

Lithic designator	Description	Interpretation
Qo	**Ocotillo Pebbly Sandstone and Conglomerate**: very coarse horizontally stratified pebbly sandstone at base (5- to 65-m thick), coarsening to very poorly sorted, sub-rounded, matrix-supported, very poorly indurated boulder conglomerate with clasts up to 1 m (20- to 30-m thick). Felsic-plutonic and gneissic clasts in the NE Mecca Hills, and Orocopia Schist clasts in the SW Mecca Hills.	Proximal to medial alluvial fan
Qpu-ms	**Upper Palm Spring Mudstone and Siltstone**: laminated claystone, mudstone, and siltstone. Occasional burrows, mottling, and gastropod fossils. Lacks desiccation features.	Shallow lacustrine
Qpu-mss	**Upper Palm Spring Mudstone, Siltstone, & Sandstone**: horizontally stratified mudstone, laminated sitlstone, and featureless to moderately normal-graded medium- to fine-grained sandstone. Lacks desiccation features.	Shallow lacustrine with coarser input from flash-flood events
Qpu-bss	**Upper Palm Spring Bedded Sandstone and Siltstone**: moderately normal-graded medium- to coarse-grained sandstone (0.2- to 1-m thick) fining to ripple cross-laminated biotite-rich green siltstone 5- to 10-cm thick. Also, horizontally stratified featureless 5- to 20-cm thick medium-grained sandstone with interbedded 5- to 20-cm thick laminated to mottled and desiccated siltstone. Burrows and root casts common.	Distal alluvial fan sheetflood deposits and nearshore to very shallow lacustrine
Qpu-pss	**Upper Palm Spring Pebbly Sandstone & Siltstone**: horizontally stratified amalgamated sheets of very coarse-grained to mildly pebbly sandstone of variable thickness with interbedded 1- cm to 1.5-m thick green laminated to ripple-cross laminated siltstone. Occasional small (~1.5-m wide, ~20-cm deep) clast-supported pebble to cobble conglomeratic channel fills. Calcic paleosols common.	Distal alluvial fan
Qpu-ps	**Upper Palm Spring Pebbly Sandstone**: horizontally stratified very coarse-grained pebbly sandstone in broad flat-based, convex-up, amalgamated sheets (5- to 40-cm thick) with pebble stringers and rounded clast-supported rounded cobble-conglomerate channel fills (<1-m thick).	Medial alluvial fan
Qpu-cg	**Upper Palm Spring Pebbly Conglomerate**: horizontally stratified, amalgamated, sub-angular, dominantly matrix-supported, cobble to boulder conglomerate. Felsic-plutonic and gneissic clasts in the NE Mecca Hills (typically <0.5 m).	Proximal to medial alluvial fan
Qpu-rc	**Upper Palm Spring Red Conglomerate**: horizontally stratified to massive, sub-angular, dominantly matrix-supported cobble to boulder conglomerate composed of entirely Orocopia schist debris.	Proximal alluvial fan
Qpl-pss	**Lower Palm Spring Pebbly Sandstone & Siltstone**: very coarse-grained to pebbly trough cross-bedded sandstone (1- to 6-m thick) with occasional cobble and interbedded 0.5- to 4-m thick laminated and ripple-cross laminated, biotite rich green medium sandstone and siltstone. Bedding is uniform and tabular, and individual beds are traceable for several km's.	Fluvial and overbank fines
Qpl-cg	**Lower Palm Spring Conglomerate**: horizontally stratified to massive, sub-angular, dominantly matrix-supported cobble to boulder conglomerate composed of mostly felsic-plutonic and gneiss clasts.	Proximal alluvial fan
Pm	**Mecca Conglomerate**: Maroon colored, poorly sorted, sub-angular to sub-rounded, cobble to small boulder conglomerate. Lower section dominated by clast supported (clasts <0.5 m) poorly developed planar bedding (<3 m thick) with sharp non-erosive bases and lacking internal sedimentary structure (except clast imbrication). Grades into dominantly matrix supported (clasts <20 cm) conglomerate, better developed bedding (<1.5-m thick) with increasingly abundant very coarse-grained small sandstone channel fills.	Proximal alluvial fan

and net SW-directed paleocurrent directions suggest that coarse gravelly deposits were derived from the northeast, likely from the northeast side of the PCF. The overall fining-up trend records a gradual reduction in coarse sediment supply and depositional energy.

4.2.2. Palm Spring Formation

The Palm Spring Formation consists of lower and upper members separated by a widespread angular unconformity (Figs. 4, 6B, 8E). The unconformity marks the boundary between regionally extensive and relatively uniform facies of the lower member, and highly variable localized facies of the upper member in the central Mecca Hills.

The lower member of the Palm Spring Formation is 340 m thick in lower Painted Canyon where it conformably and gradationally overlies the Mecca Formation on the SW limb of Mecca Anticline (Figs. 3, 4, 6B). It consists of tabular, uniformly bedded couplets of grus-rich, cross-bedded pebbly sandstone with plutonic and gneissic composition that fine up into biotite-rich ripple cross-laminated green siltstone and fine-grained sandstone to siltstone (Table 1, Fig. 7B). Individual beds are laterally continuous with sharp boundaries that are traceable for several kilometers along strike, typically with little change in facies. Paleocurrent indicators suggest SE-directed transport (Fig. 6B). The lithofacies assemblage and stratal architecture of the lower member in the central Mecca Hills is similar to that seen in the Indio Hills 25 km to the northwest, providing evidence for its regional extent. Exceptions are observed in Eagle Canyon where the lower member consists of poorly sorted cobble to boulder conglomerate (Table 1), and in the southeast part of the study area near Hidden Spring Wash (Fig. 2) where similar coarse facies were previously documented (Chang et al., 1987; Boley et al., 1994).

The laterally extensive architecture and uniform facies of the lower member suggest deposition in a fluvial system composed of a migrating main channel or multiple channels (cross-bedded sandstone) and adjacent overbank floodplain (ripple cross-laminated green siltstone) that occupied a broad basin floor. The unconfined lateral migration of river channels created tabular-bedded fluvial architecture (e.g., Miall, 1985; Hampton and Horton, 2007). Felsic-plutonic and gneissic clast compositions, and SE-directed paleocurrents suggest that the lower member was deposited in a large river system that flowed SE down the paleo-Coachella Valley into the Salton Trough, with sediment sources mainly in the Cottonwood and Little San Bernardino Mountains. Localized coarse facies of the lower member likely were deposited in proximal basin-margin alluvial fans.

The upper member of the Palm Spring Formation contains a wide range of lithofacies types that display abundant vertical and lateral variability, in contrast to the regionally uniform nature of the lower member. Despite the contrast in deposits across the PCF, we recognize a distinct and laterally extensive limestone bed (LM) that correlates from northeast of the PCF near Eagle Canyon (110 m section 1, Figs. 3, 4, 6A, 9A) to southwest of the PCF in Painted Canyon (635 m section 3, Figs. 3, 4, 6B, 9C). This ~3-m-thick bed is characterized by horizontally stratified ~1- to 5-cm thick beds of platy white limestone interbedded with thin (<5-mm) laminated green siltstone in the lower ~1.5 m that coarsen to >10-cm-thick medium sandstone interbeds in the upper ~1.5 m. Limestone beds consist of ~3-mm thick-flakey calcite laminae (possibly varves) with rare burrows, and abundant calcareous bladed fossil plant material that appears to be matted grasses (Figs. 9B, D). Correlation of the limestone across the PCF is based on its unique and laterally persistent lithologic characteristics, and its stratigraphic position ~80–90 m above an angular unconformity both northeast and southwest of the PCF (Figs. 4, 6).

Southwest of the PCF in lower Painted Canyon, the upper member of the Palm Spring Formation is >700 m thick and fines up-section from coarse conglomeratic sandstone with channel-fill conglomerate to very coarse-grained planar and cross-bedded pebbly sandstone and

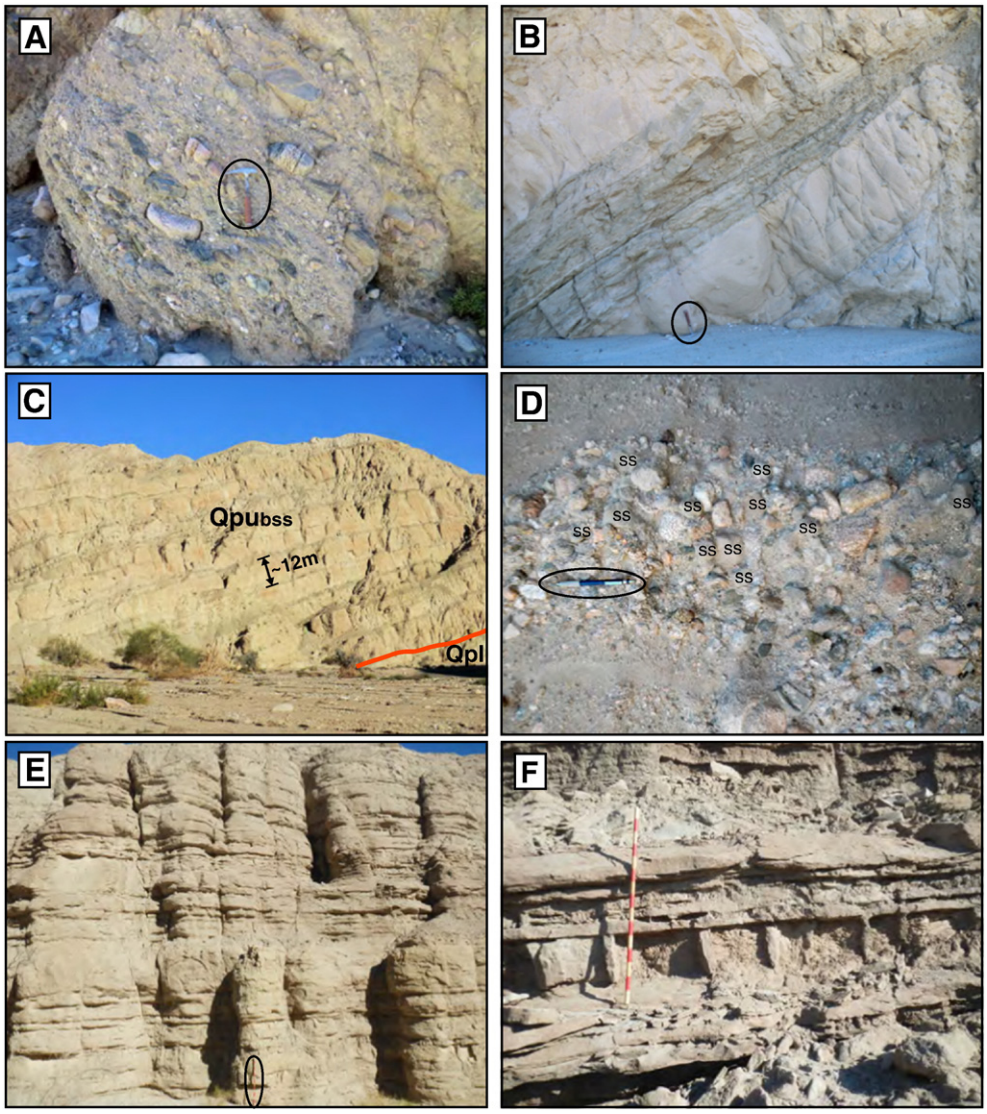

Fig. 7. Photographs of sedimentary rocks exposed in the Mecca Hills. (A) Mecca Conglomerate in lower Painted Canyon. Hammer circled for scale. (B) Fining-up sequence from pebbly sandstone to siltstone in the lower member of the Palm Spring Formation. Hammer circled for scale. (C) Interbedded pebble–cobble sandstone and siltstone of the upper member of the Palm Spring Formation (Qpu) exposed in Box Canyon. Red line indicates angular unconformity separating the upper and lower (Qpl) members. (D) Conglomerate in upper member of the Palm Spring Formation, NE of the PCF, with abundant clasts of sandstone reworked from the lower member. (E) Medium-bedded sandstone and siltstone of the upper member northeast of the PCF (1.5-m Jacob's staff circled). (F) Thinly-bedded sandstone with desiccated siltstone and mudstone of the upper member northeast of the PCF. 1.5-m Jacob's staff for scale.

interbedded green ripple-cross-laminated siltstone (Fig. 7C), with the abundance of siltstone interbeds increasing up-section (Table 1, Fig. 6B). Thin coarsening-up intervals (0.5–1.5 m) of claystone to medium-grained sandstone are more abundant above 860 m in section 3 (Fig. 6B). Imbricated clasts, channel scours, cross-bedded foresets, tool marks, and flute casts all indicate paleoflow to the SSW to SSE (Fig. 6B).

The coarsest facies of the upper Palm Spring member southwest of the PCF suggest deposition in a proximal to distal alluvial-fan system (e.g., Blair, 1987a). Higher in the section (Fig. 6B), horizontally stratified and cross-bedded coarse-grained sandstone and siltstone may represent a transition to distal-alluvial-fan to fluvial environments (e.g., Nichols and Hirst, 1998) near the margin of a paleo-lake in the Salton Trough. The thin coarsening-up intervals of claystone and medium-grained sandstone are inferred to record short-lived lake highstands followed by rapid SE progradation of distal alluvial fans into the lake.

Northeast of the PCF, the base of the upper Palm Spring member near Eagle Canyon consists of locally preserved, channelized red cobble-boulder conglomerate. This conspicuous conglomerate is exposed on the southwest side of Eagle Canyon at the contact between the lower and upper members, and resembles similar conglomerates above the unconformity in the southeast Mecca Hills (e.g., Chang et al., 1987; Sheridan and Weldon, 1994). The unit is typically less than ~30-m thick with a scoured base and contains exclusively Orocopia Schist clasts with SW-directed paleocurrent indicators (Fig. 6A). A cobble-lag cap separates it from more uniform and widely distributed sandstone facies described above (Table 1, Figs. 4, 6A).

Very coarse deposits of the upper member exposed in upper Painted Canyon consist of horizontally stratified pebble-cobble conglomerate that grade laterally into planar amalgamated, very coarse-grained pebbly sandstone (Table 1, Fig. 8B). Calcic paleosols and laterally extensive ~0.5- to 2-m thick heavily desiccated red mudstone beds with sharp bases are intermittently interbedded with the coarser facies of the upper member (Fig. 8C). Clasts are dominantly felsic-plutonic and gneiss. In addition, the first clasts of reworked sandstone in

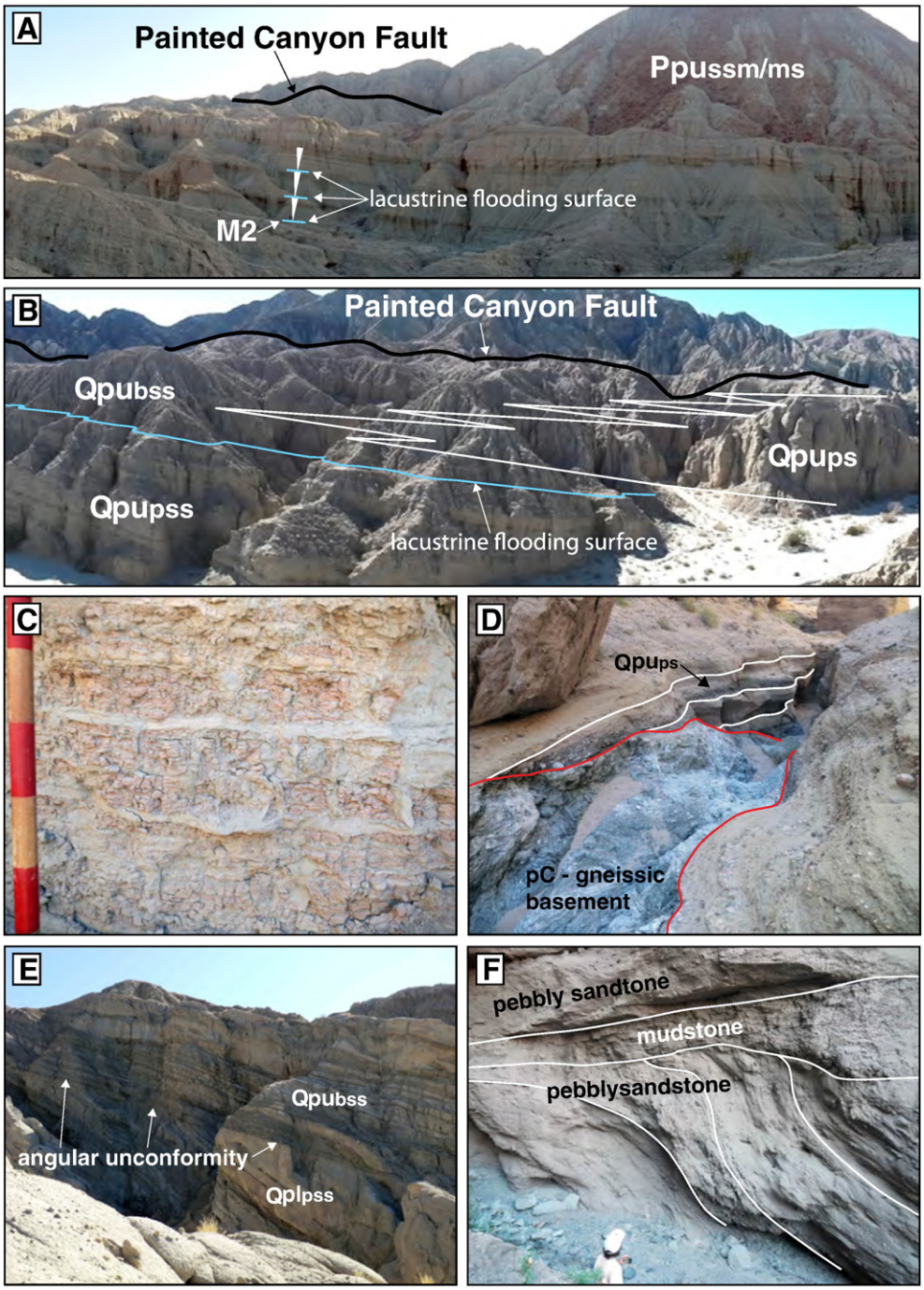

Fig. 8. Photographs of stratigraphic relationships in the Mecca Hills. (A) Coarsening-up sequences in lacustrine and nearshore deposits capped by lacustrine flooding surfaces between Eagle Canyon and the PCF. (B) Medial alluvial fan deposits (Qpu-pss) capped by lacustrine flooding surface and lateral interfingering of nearshore bedded sandstone and siltstone (Qpu-bss) with distal alluvial fan deposits (Qpu-ps) of the upper member of the Palm Spring Formation. (C) Sandstone-filled mudcracks in desiccated mudstone of marker horizon M10a. 10-cm-long divisions on Jacob's Staff for scale. (D) Upper member of the Palm Spring Formation onlapping basement northeast of the PCF. (E) Angular unconformity separating lower from upper Palm Spring Formation near Box Canyon. (F) Angular truncation of sandstone beds capped by mudstone in the upper member of the Palm Spring Formation northeast of the PCF.

conglomeratic channel fills are observed several meters beneath marker horizon M10a (Figs. 7D, 6A), within 280-m map distance northeast of the PCF (Fig. 4). While other sandstone clasts likely sourced from the Miocene Diligencia basin to the east (Law et al., 2001; Ingersoll et al., 2014) have been found in the Palm Spring Formation, we infer that these sandstone clasts were eroded from the lower member of the Palm Spring Formation because of their compositional and textural similarity to the lower member, and their proximity to the PCF. Imbricated clasts in the upper member in upper Painted Canyon record consistent SE paleoflow, roughly parallel to the trace of the PCF (Figs. 4, 6A).

Medium-grained facies of the upper member comprise two distinct variants of bedded sandstone and siltstone. The first consists of well bedded, normally graded sandstone (0.2- to 1.5-m thick) with thin (1- to 5-cm thick) interbedded siltstone (Fig. 7E); the other consists of bedded internally structureless sandstone (5- to 20-cm thick) with interbedded desiccated siltstone and mudstone (4- to 50-cm thick) (Table 1, Fig. 7F). The finest-grained facies are preserved as 20- to 30-m-thick coarsening-up sequences of laminated claystone, mudstone, siltstone, and coarse-grained sandstone low in section 1 near Eagle Canyon, adjacent to the PCF (Table 1, Fig. 8A). In northwestern-most upper Painted

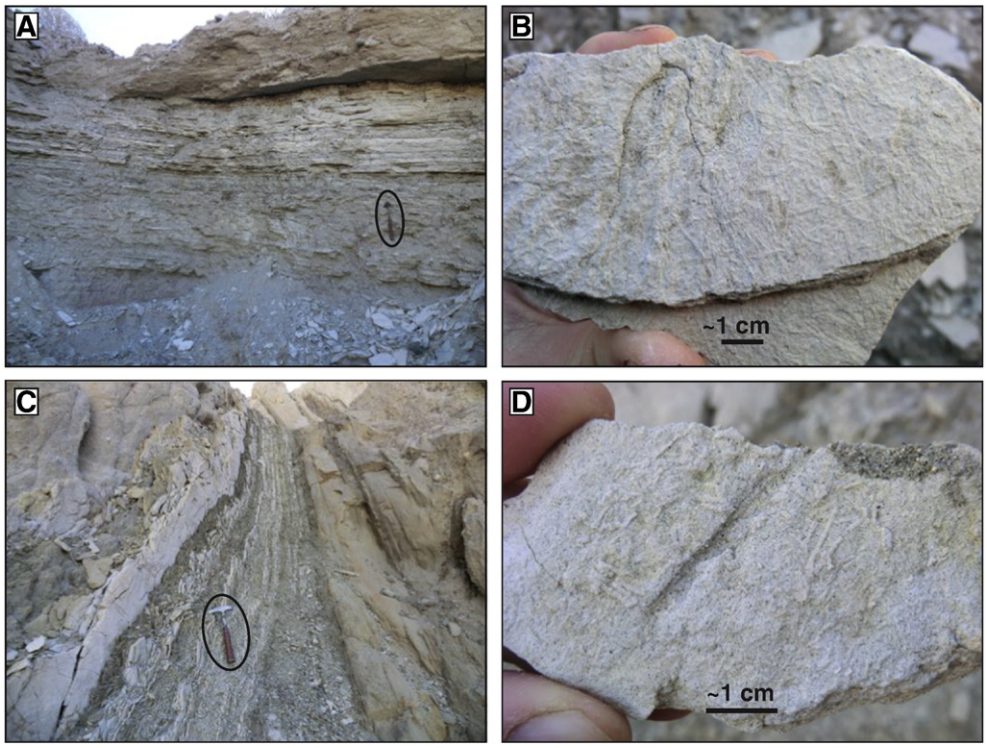

Fig. 9. Field photos of the limestone marker horizon LM A) northeast of the PCF near Eagle Canyon (hammer circled for scale) with B) hand sample, and C) southwest of the PCF near lower Painted Canyon (hammer circled for scale) with D) hand sample.

Canyon, similar fine-grained facies comprise a ~200-m fining-up sequence from laminated siltstone to mudstone to claystone adjacent to the PCF splay (Figs. 4, 6A).

We infer that the red basal conglomerate was deposited during a brief episode of SW-directed transport in alluvial fans derived from local Orocopia Schist sources, during and/or immediately after intrabasinal to regional folding and transpressive deformation that created the unconformity between the lower and upper Palm Spring members. Coarse pebble conglomerate and pebbly sandstone of the upper member northeast of the PCF were deposited in the medial to distal reaches of alluvial fans (e.g. Blair and McPherson, 1994), that were transported to the SE. Rapid lateral fining of horizontally stratified conglomerate to planar pebbly sandstone with reworked conglomeratic channels is consistent with down-transport facies associations observed in active alluvial fans (Blair, 1987a). Clast compositions and SE-directed paleocurrent indicators suggest the fans were sourced from the Cottonwood Mountains (Fig. 1). The thicker normally graded sandstone and siltstone variants (Fig. 7E) are interpreted as sheetflood deposits that accumulated in distal-alluvial-fan and sand-flat settings (e.g., Blair and McPherson, 1994). The thinner featureless sandstone, siltstone, and mudstone facies (Fig. 7F) are interpreted as near-shore mudflat deposits that accumulated at the most distal reaches of alluvial fans. In this setting, sheet sands were deposited by flash floods on a mudflat or in very shallow water by hyperconcentrated grain flows (e.g., Mulder and Alexander, 2001). The finest-grained facies were likely deposited by suspension settling in a shallow lacustrine environment based on dominance of laminated fine-grained mud and silt and lack of desiccation features.

4.2.3. Ocotillo Conglomerate (Qo)

The Ocotillo Conglomerate ranges in thickness from ~5 to >65 m and consists of very coarse-grained, horizontally stratified sandstone that coarsens up section to poorly sorted pebble-cobble- to small-boulder conglomerate (Table 1). Clast compositions are entirely felsic-plutonic and gneissic with SW-directed paleocurrent indicators in the northwest and northeast Mecca Hills (Fig. 6A). Southwest of the SAF northwest of Painted Canyon, Ocotillo Conglomerate consists of large, several-km-wide, overlapping units of horizontally stratified conglomeratic sandstone with two distinct compositions: (1) felsic-plutonic and gneissic clasts and (2) almost entirely Orocopia Schist clasts. In the southeast Mecca Hills different conglomerate facies interfinger with the Palm Spring Formation and persist intermittently up to the modern alluvial fans. While the latest progradation of these fans may be linked to Ocotillo Conglomerate progradation, the Ocotillo is generally considered an older (Pleistocene) lithostratigraphic unit.

The erosional base and widespread thin-sheet-like geometry of the Ocotillo Conglomerate records basinward progradation of gravels shed from nearby mountains. In the northeast Mecca Hills this unit represents the gravelly deposits of a SW-transported alluvial-fan system sourced in the Cottonwood Mountains, northeast of the Mecca Hills (Fig. 2). Southwest of the San Andreas fault, the Ocotillo Conglomerate likely has been translated a significant distance northwest by dextral slip from its original depositional location. Here, the alternation of contrasting clast compositions and basin-ward paleocurrent indicators suggest that the Ocotillo Conglomerate was deposited in overlapping alluvial fans sourced from the Cottonwood Mountains (felsic-plutonic clast source) and Orocopia Mountains (schist clast source).

4.3. Stratigraphic and basinal architecture

4.3.1. Northeast of the Painted Canyon fault

Facies associations of the upper member northeast of the PCF in the central Mecca Hills exhibit a retrogradational architecture that defines a lacustrine transgression from SE near Eagle Canyon to NW in upper Painted Canyon (Fig. 4). Lacustrine deposits near Eagle Canyon, adjacent to the PCF (Fig. 8A) coarsen rapidly to the northwest into laterally equivalent distal and medial alluvial-fan facies (Fig. 8B). Abrupt lacustrine flooding surfaces topped by sub-meter-thick desiccated mudstone beds (Fig. 8C) interrupt these coarser facies and record the persistent, fluctuating lake to the SE. The gradual fining-up lacustrine sequence high in section 1, located at the northwest end of upper Painted Canyon (Figs. 4, 6A 10A), records a shift of the lacustrine depocenter to the NW

across a distance of ~4.5 km relative to the oldest lacustrine deposits near Eagle Canyon.

Sylvester and Smith (1976) noted the relatively thin upper Palm Spring member northeast of the PCF, where it dips modestly (<14°) and rests on intermittently exposed shallow basement (Fig. 8D). Section 1 (Fig. 6A) shows that despite low bedding dips and shallow basement, the upper member is ~800 m thick northeast of the PCF, which requires low-angle onlap of the upper member onto basement (Fig. 10B). Although the mechanism that created accommodation is uncertain, it may be related to gentle syn-depositional tilting and translation of deposits along the PCF away from a fixed structural depocenter, similar to Ridge Basin (e.g. Crowell, 2003).

4.3.2. Southwest of the Painted Canyon fault

The contact between the lower and upper members of the Palm Spring Formation is generally known throughout the Coachella Valley as a prominent, widespread angular unconformity that varies from high- to low-angle (e.g., Boley et al., 1994). Detailed mapping near lower Painted Canyon reveals that the angular unconformity in this area is a laterally discontinuous, time-transgressive surface. The contact changes over several kilometers along strike from a high-angle unconformity near the southwest entrance of Box Canyon (Fig. 8E) to a laterally equivalent conformable surface 3.2 km northwest at Painted Canyon, where the surface is stratigraphically within the upper part of the lower Palm Spring member (~553 m in section 3; Figs. 6B, 11). This surface is 117 m stratigraphically beneath a similar horizon mapped from the northwest, where a second, younger angular unconformity at the lower-upper Palm Spring contact is observed 1 km northwest of Painted Canyon (Figs. 6B, 11).

The configuration of this time-transgressive unconformity is delineated by mapping of the marker limestone bed, LM (Fig. 9), which lies stratigraphically between the two unconformities and their laterally equivalent conformable surface in the area between lower Painted Canyon and Box Canyon (Fig. 11). This relationship implies that there are at least two distinct angular unconformities separating the lower and upper Palm Spring Formation in this area, and the lower and upper members between the two unconformities are lateral equivalents in the area of lower Painted Canyon (Figs. 11, 12). Estimates of stratigraphic thickness based on bedding attitudes and map distance indicate thickening of the stratigraphic interval between the two unconformities from ~117 m at lower Painted Canyon to ~230 m at a location 2.25 km SE of lower Painted Canyon (Figs. 11, 12). This architecture provides evidence for coeval sedimentation and intrabasinal tilting during this phase of deformation.

4.4. Stratigraphic ages and sediment-accumulation rates

4.4.1. Measured section 1

Measurement and analyses of the paleomagnetic data found that the majority of the samples have well-defined magnetization components, with the characteristic magnetization being defined by 550° to 680° thermal steps (Fig. 13). A minority of the samples had less-well defined components that were not useful for principle-component analysis (PCA), but that could be used to determine polarity - these are noted as "c2" sites in Table DR-1. Finally, a small number of sites had results that were too poorly defined to determine polarity - these are noted as "i" sites in Table DR-1. Best fit lines from PCA were used to determine sample-level directions, site means, and calculation of VGP latitude (Table DR-1). Because the bedding attitudes within section 1 have very little variation, and shallow dips, paleomagnetic fold tests are not conclusive. Positive reversals tests (Messé, 2014; Dimitroff, 2015), and stratigraphically coherent polarity zones do suggest a depositional age of the magnetizations obtained from this section.

Our paleomagnetic sampling of section 1 consists of 82 sites that yield 7 magnetic reversals and 8 magnetochrons (Figs. 6A, 14). The Bishop Ash high in the section (projected into section 1; Fig. 6A) is an important marker that permits identification of the normal-polarity Brunhes magnetochron (0.78 Ma to present). A reversal between 856 and 841 m in section 1 is inferred to be the Brunhes–Matuyama boundary, based on our projection of the nearby 0.76-Ma Bishop Ash into the section (Figs. 4, 6A). Below this level, section 1 contains most of the reversed-polarity Matuyama magnetochron, including the normal-

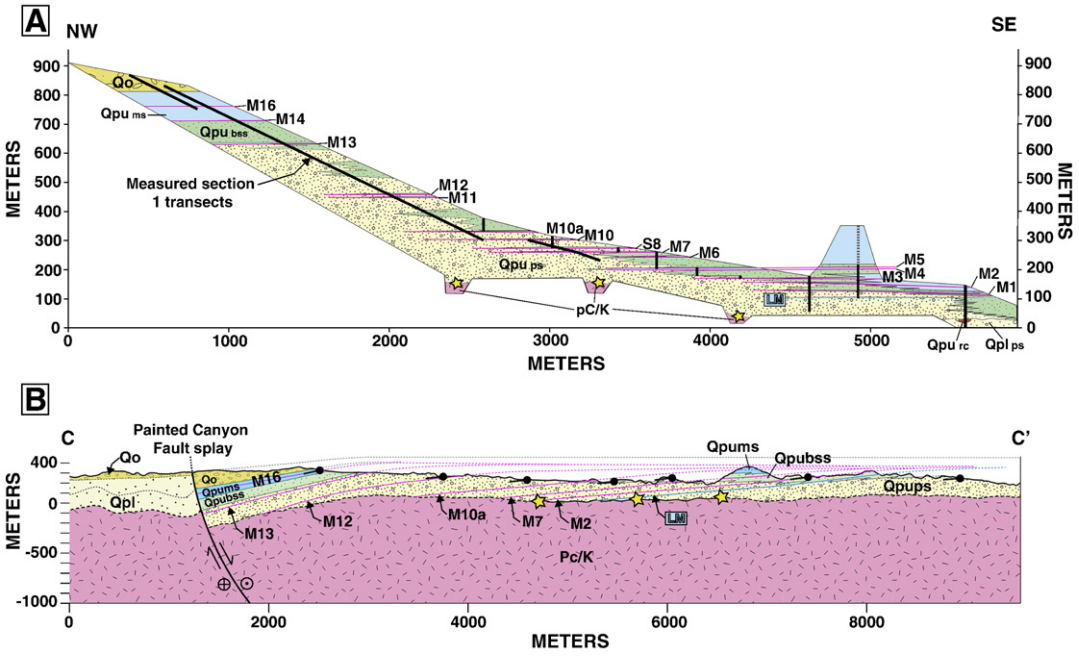

Fig. 10. NW to SE sections northeast of the PCF. LM is limestone marker horizon. Marker horizons used to correlate measured section 1 shown as pink lines and labeled (e.g. M2). Stars represent calculated depth to-basement projected into section from nearby sediment–basement contacts. (A) Facies panel for section 1 showing northwest transgression of lacustrine mudstone and siltstone (Qpums) and nearshore sandstone and siltstone (Qpubss) over distal alluvial fan pebbly sandstone (Qpups) though time. (B) Geologic cross section line C–C′ in Fig. 4 on the northeast side of the PCF. Bedding dips and shallow basement requires low-angle down-lapping relationship of sedimentary rocks onto basement. Wedging of Ocotillo Conglomerate against transtensional Painted Canyon fault splay shown.

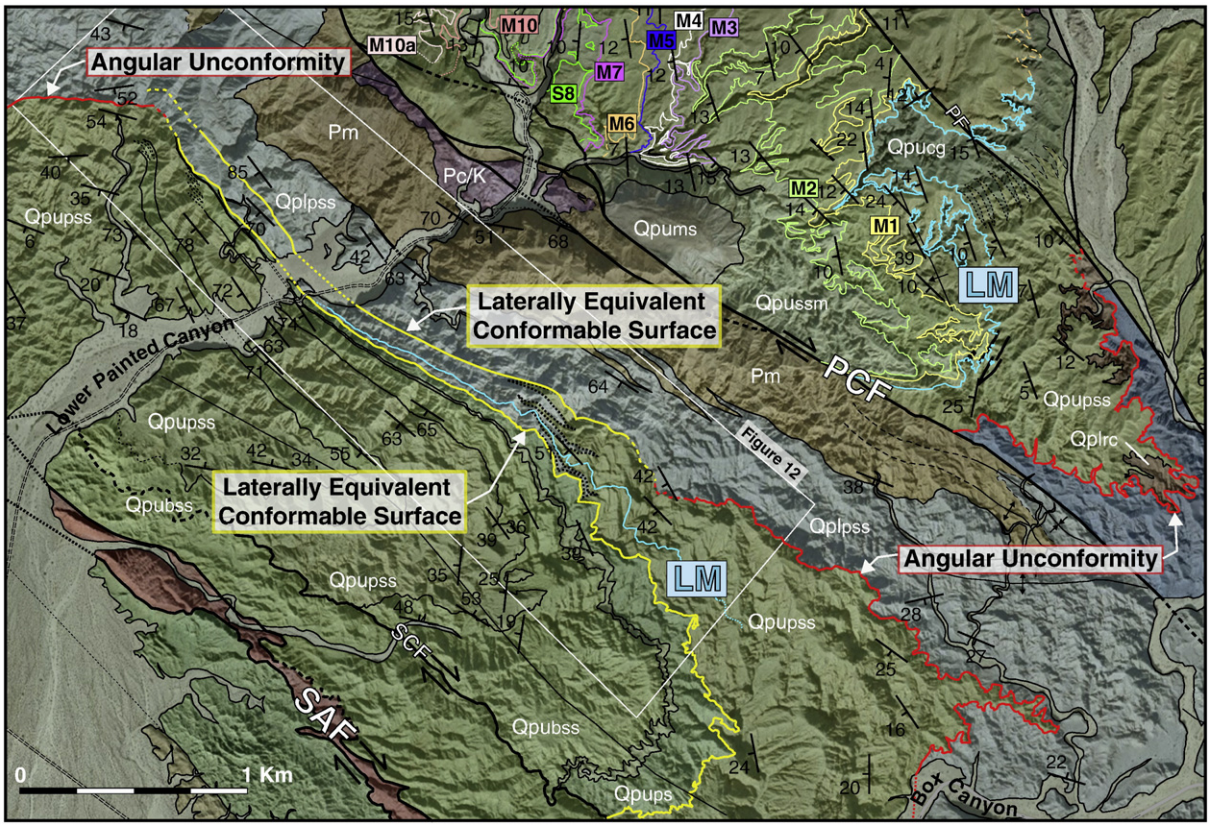

Fig. 11. Detailed geologic map of a portion of the study area (see location in Fig. 4) showing distribution of numbered marker beds NE of the PCF, and two time-transgressive angular unconformities SW of the PCF that separate the lower and upper members of the Palm Spring Formation. The two unconformities (red lines) can be mapped along strike into laterally equivalent conformable surfaces (yellow lines). Deposits stratigraphically between the two unconformities SW of the PCF comprise a SE thickening wedge of laterally interfingering lower and upper members of the Palm Spring Formation. Limestone marker unit LM correlates from section 1 NE of the PCF to the interval between the two unconformities SW of the PCF, thus providing control on the age of the unconformities.

polarity Jaramillo, Olduvai, and Reunion subchrons (Figs. 6A, 14). Using the minimum and maximum possible stratigraphic positions of reversals in section 1, and their ages, we calculate a range of sediment accumulation rates (Table 2). We assume a constant sedimentation rate for strata beneath the Reunion by extrapolating the upper Olduvai to lower Reunion rate (0.51 mm/yr) to the base of the upper Palm Spring member. The minimum (0.27 mm/yr) and maximum (0.77 mm/yr) rates from section 1 are used to define uncertainty. The resultant ages are ca. 2.4 Ma (2.6–2.3 Ma) for the LM marker, and ca. 2.6 Ma (3.0–2.4 Ma) for the base of the upper Palm Spring member, with a preferred range of 2.6–2.4 Ma for the base of the upper Palm Spring member due to the lack of normal-polarity sites that would indicate the Matuyama–Gauss reversal (2.58 Ma).

The two lowest sites in section 1 (sites 14–19 and 14–20, Figs. 6A, 14), which are reversed-polarity, were sampled beneath the angular unconformity separating the lower and upper Palm Spring members. An uncertain amount of time is represented by the unconformity, and several possibilities can explain the site polarities: (1) the unconformity

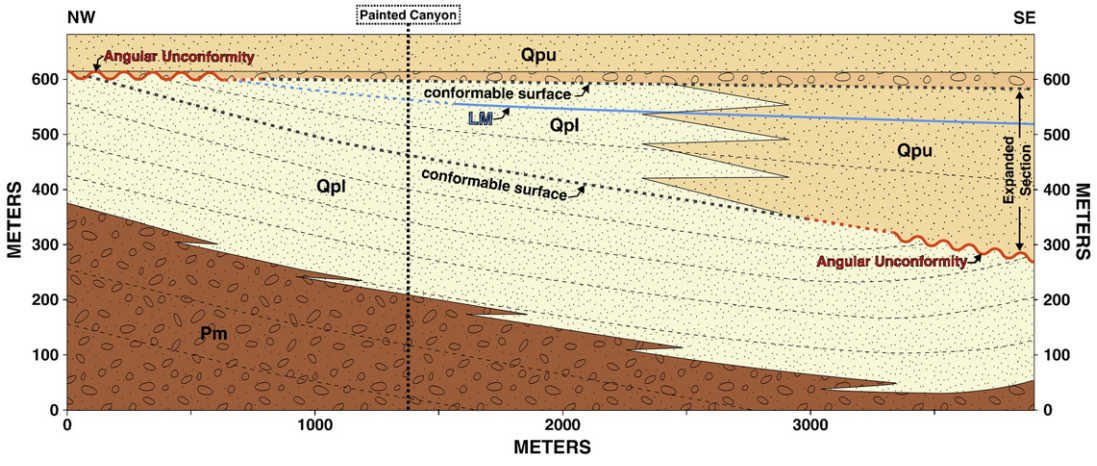

Fig. 12. Simplified diagram illustrating the stratigraphic relationships in Fig. 11 from northwest to southeast across Painted Canyon. Prominent lower unconformity in the southeast maps into a laterally equivalent conformable surface in the northwest. Upper unconformity in northwest maps into a laterally equivalent conformable surface in southeast. Intermediate southeast-thickening growth wedge of laterally interfingered lower and upper Palm Spring Formation between unconformities. Limestone bed LM is within intermediate growth wedge.

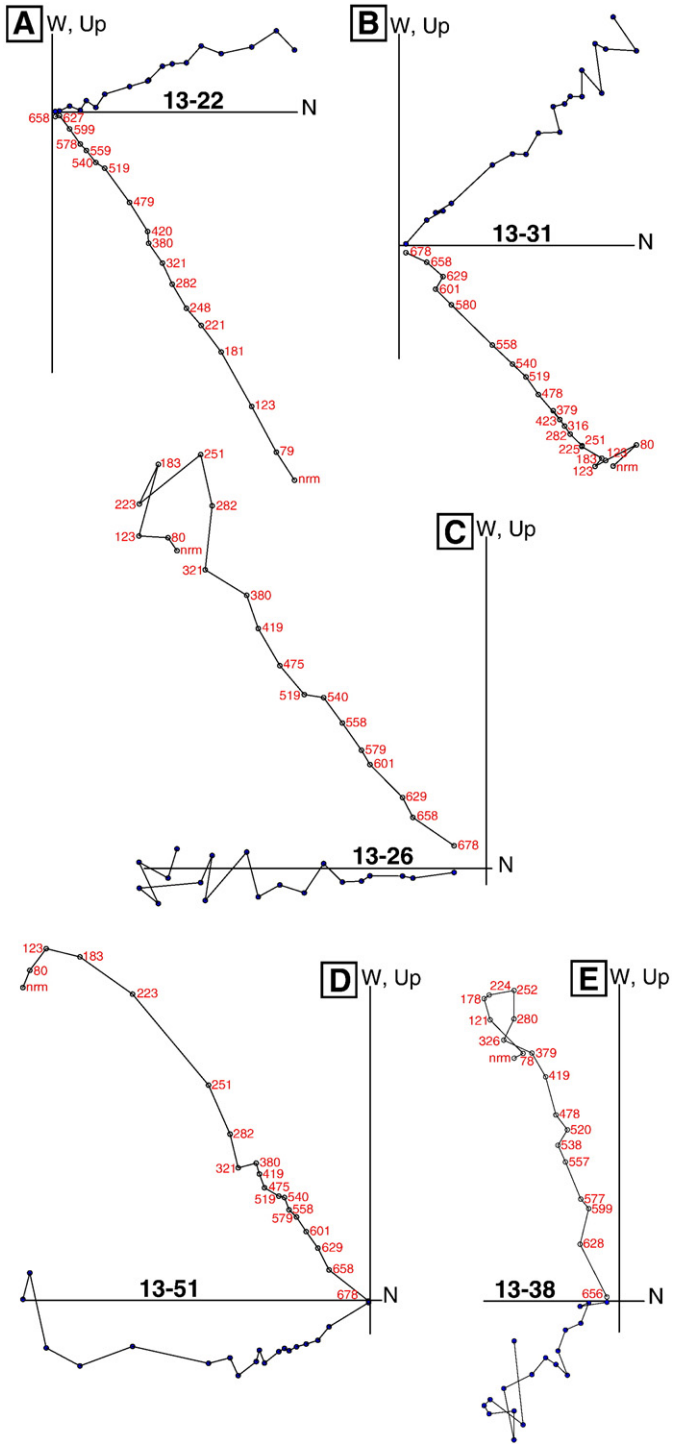

Fig. 13. Orthogonal vector plots of representative demagnetization results. All plots in tilt-corrected coordinates. Open symbols with temperature steps are vertical projection of vector on specified plane, solid symbols are horizontal projection. (A), (B), (C), results from Palm Spring Fm., section 1. (D), result from Palm Spring Fm. and (E), result from Mecca Fm., section 3.

represents little time and the two sites represent a continuation of the lowermost Matuyama magnetochron; (2) the unconformity represents significantly more time and the two sites represent the reversed-polarity Kaena or Mammoth subchrons of the Gauss, or the uppermost Gilbert magnetochron (Fig. 14); or (3) the sites have experienced reversed-polarity overprint. The progressive unconformity in section 3 that spans 200–500 m (=0.4–1.0 Myr assuming 0.5 mm/yr of accumulation) and evidence for sediment bypass near Eagle Canyon in section 1 lead us to suggest that the unconformity represents more time (option 2 above) and that sites below the unconformity represent an older reversed-polarity subchron (Fig. 14), though we cannot rule out magnetic overprint. Chang et al. (1987) suggested an age of ~2.0 Ma for the base of the upper Palm Spring member (~0.4–1.0 Myr younger than our estimate in section 1) ~5 km to the southeast near Box Canyon (Fig. 2), which further supports that the unconformity represents more time.

4.4.2. Measured section 3

As with the samples collected from section 1, samples from section 3, including the Mecca Fm, have well-defined magnetizations (Fig. 13). Analyses of these data were made using the same methodology as used for the section 1 samples. Bedding tilts within section 3 are very steep, with similar dip-directions - which also result in inconclusive fold tests. Site mean directions in in-situ coordinates are primarily down, with southerly declinations. Correcting for bedding tilt results in directions that predominantly are southerly and up, with no indication of any sites with normal polarity. An exception are the sites from the lower-most 100 m of the section - these sites have directions that are northerly and up after tilt-correction, but are southerly and up in in-situ coordinates. For further analysis of these directions, we use the in-situ directions for the sites from the lower-most portion of the section, and tilt-corrected results for the remainder of the section. All 58 sites yielded reversed polarities (Fig. 6B). We would expect section 3 to contain some of the reversals recorded in section 1 because of its greater stratigraphic thickness and presence of the ~2.4-Ma LM limestone correlated from section 1 (Fig. 6). This suggests two leading possible interpretations that we have constructed as two scenarios below.

4.4.2.1. Scenario 1. A predominantly reversed-polarity section could be obtained if the section spans the lower portion of the Jaramillo chron, which would place the boundary between the Gauss and Matuyama magnetochrons (2.58 Ma), just below the base of the sampled section. We can estimate the sediment-accumulation rate from this reversal to limestone unit LM. However, the uncertainty in our age estimates for LM overlaps the age of the Gauss-Matuyama magnetochron reversal, resulting in a sediment-accumulation rate for the ~620 m of section ranging from instantaneous deposition to ~2.2 mm/yr. This wide range of possible sediment-accumulation rates hinders our ability to estimate ages for stratigraphic boundaries in section 3. Assuming the Gauss-Matuyama reversal may be located just below the base of the section, a minimum sediment-accumulation rate of ~0.7 mm/yr (not included in the above-stated estimate range) would be required to deposit the section from just below the base of the section to the top of the section (at 1300 m) within the mostly reversed-polarity Matuyama. This would imply that all three normal-polarity subchrons (Jaramillo, Olduvai, and Reunion), which represent 14% of the Matuyama magnetochron time, were missed by our sampling. Because this is unlikely, we favor scenario 2.

4.4.2.2. Scenario 2. Alternatively, the dominance of magnetically reversed sites in section 3 may result from a reversed-polarity remagnetization event during the late Matuyama magnetochron. Section 3 is located on the steeply dipping limb of a tight syncline between the Painted Canyon and San Andreas faults, and has experienced more deformation than strata of section 1. It also is located in a deeper structural block than section 1, so has potentially been subjected to greater fluid flow (and related cementation) from the Coachella Valley aquifer system compared to deposits northeast of the PCF. We therefore tentatively attribute the remagnetization to some combination of diagenesis and weak pressure solution of clay minerals (e.g., Housen et al., 1993), and/or fluid flow associated with deformation (e.g. Katz et al., 1998, Elmore et al., 2006). In this case we estimate contact ages by extrapolating sediment accumulation rates from the 2.6–2.3 Ma LM horizon using

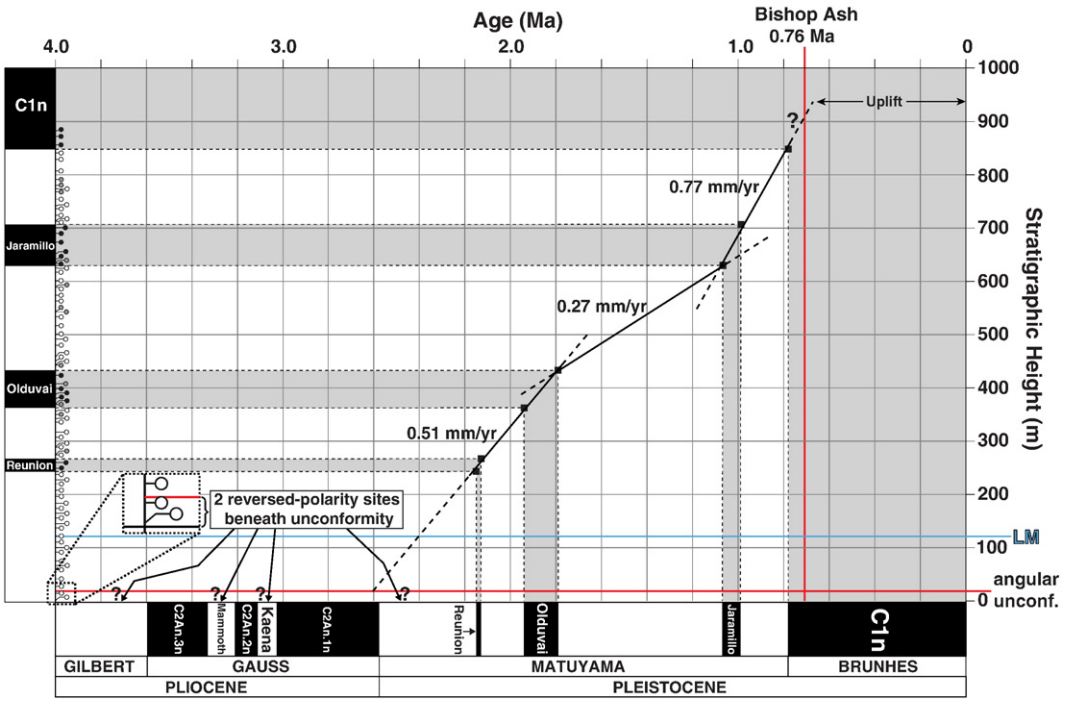

Fig. 14. Correlation between polarity zones of section 1 and geomagnetic polarity timescale, with average and projected sediment accumulation rates.

an average rate calculated from section 1 (0.5 mm/yr). Using this method we estimate an age range of 5.0–3.1 Ma (3.7 Ma preferred) for the base of the Mecca Conglomerate, 3.7–2.7 Ma (3.0 Ma preferred) for the base of the lower Palm Spring member, 2.9–2.4 Ma (2.6 Ma preferred) for the lower unconformity, 2.6–2.2 Ma (2.3 Ma preferred) for the upper unconformity (base of the upper Palm Spring member), and 1.7–0 Ma (1.1 Ma preferred) for the top of the section. We tentatively use scenario 2 to estimate ages for section 3. Stratigraphic age estimates reported below carry uncertainties of ~0.5–1 Myr.

5. Discussion

5.1. Paleogeographic and fault reconstructions

The data presented above allow us to reconstruct the paleogeography of the central Mecca Hills and surrounding areas by tracking migration of depocenters and structurally controlled sub-basins through time (Figs. 15, 16). Prior to deposition of the Mecca Conglomerate, the central block was not accumulating sediment and basement rock likely was exposed and eroding at the surface. Beginning ca. 3.7 Ma, subsidence of the central block lead to deposition of the Mecca Conglomerate in SW-directed alluvial fans sourced from uplifted basement of the platform block (Fig. 15A). The presence of thick Mecca Conglomerate southwest of the PCF and its absence northeast of the fault suggests that SW-side down slip on the PCF lead to subsidence of the central block and uplift of the platform block (Fig. 16A). Systematic fining-up in the upper Mecca Conglomerate records a transition to regional subsidence and deposition of basinal fluvial environments over fault-bounded alluvial fans. Retreat and submergence of alluvial fans by finer-grained fluvial deposits likely was controlled by cessation of slip on the PCF, and either a decrease in the rate of sediment delivery or an increase in subsidence rate, or possibly both (e.g., Heller and Paola, 1992; Paola et al., 1992; Gordon and Heller, 1993).

The lower member of the Palm Spring Formation was deposited on both sides of the PCF in a large SE-directed fluvial system beginning ~3.0 Ma (Fig. 15B). The persistent, regionally observed facies and extensive lateral stratigraphic architecture, and lack of evidence for syntectonic deposition (unconformities, growth strata, etc.), implies regional subsidence and sedimentation and relative quiescence of the PCF (Figs. 15B, 16B) during this time interval. The tabular sheet-like

Table 2
Calculated sediment-accumulation rates based on magnetic reversal ages and stratigraphic thickness from section 1.

Stratigraphic interval	Time interval (Ma)	Duration of interval (ky)	Minimum interval thickness (m)	Maximum interval thickness (m)	Minimum sedimentation rate (mm/yr)	Maximum sedimentation rate (mm/yr)	Uncertainty (mm/yr)
Base of Brunhes to top of Jaramillo	0.78–0.99	210,000	128	155	0.6	0.7	0.1
Top of Jaramillo to base of Jaramillo	0.99–1.07	80,000	67	87	0.8	1.1	0.2
Base of Jaramillo to top of Olduvai	1.07–1.79	720,000	184	211	0.3	0.3	0.1
Top of Olduvai to base of Olduvai	1.79–1.94	150,000	54	86	0.4	0.6	0.1
Base of Olduvai to top of Reunion	1.94–2.13	190,000	67	95	0.4	0.5	0.1
Top of Reunion to base of Reunion	2.13–2.15	20,000	11	37	0.6	1.9	0.7

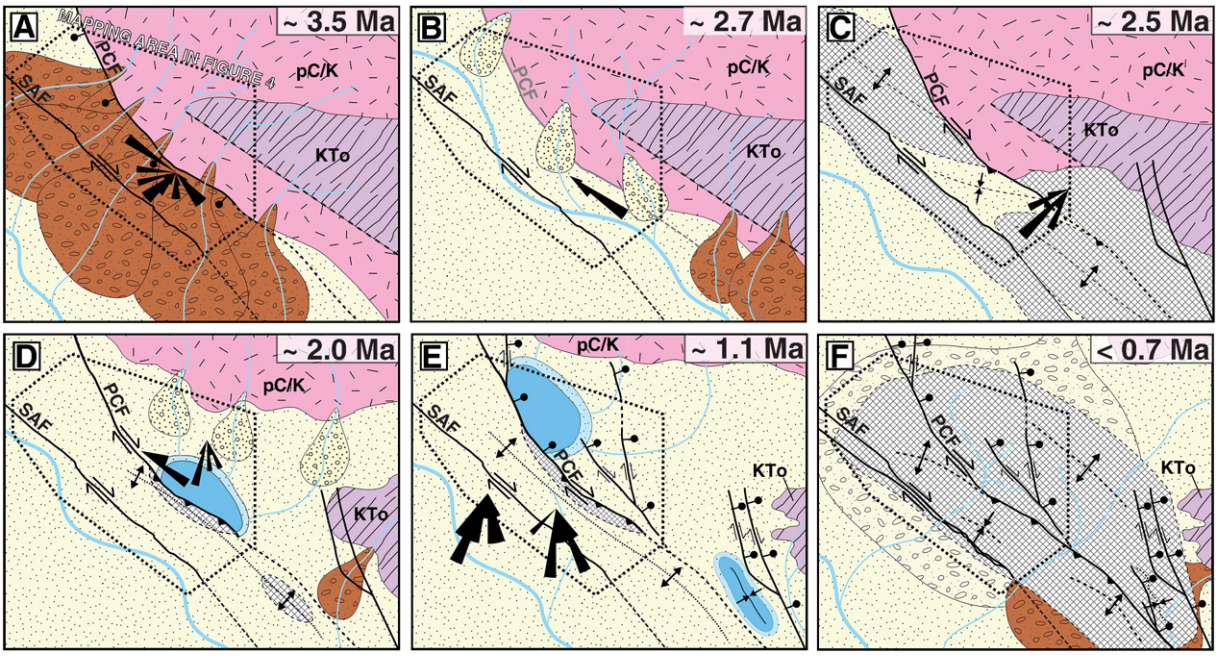

Fig. 15. Paleogeographic reconstructions of the Mecca Hills from ~3.5 Ma to the present. (A) Initiation of southwest-side down slip on the PCF and deposition of the Mecca Conglomerate between ~3.1 and 5.0 Ma. (B) From 3.0–2.6 Ma a southeast-directed fluvial system deposited the lower member of the Palm Spring Formation across the alluvial fans of the Mecca Conglomerate and the PCF. (C) At ~2.6 Ma southwest-side up slip on the PCF resulted in deformation of the basin. (D) By ~2.0 Ma a lake system was established northeast of the PCF due to pooling of water against a topographic high along the PCF. (E) At ~1.1 Ma initiation of the transtensive PCF splay shifted the lake depocenter to the northwest. (F) post-700-ka uplift and erosion of the Mecca Hills shortly after deposition of the Ocotillo Conglomerate from progradation of gravel from the Cottonwood and Orocopia mountains.

architecture of alternating sandstone and siltstone units suggests that the lower member accumulated in a wide river valley with dimensions similar to those of the modern Coachella Valley (Figs. 1, 15B, 16B).

The angular unconformity between the lower and upper members of the Palm Spring Formation in the central Mecca Hills records the onset of deformation, erosion, and a major structural reorganization of

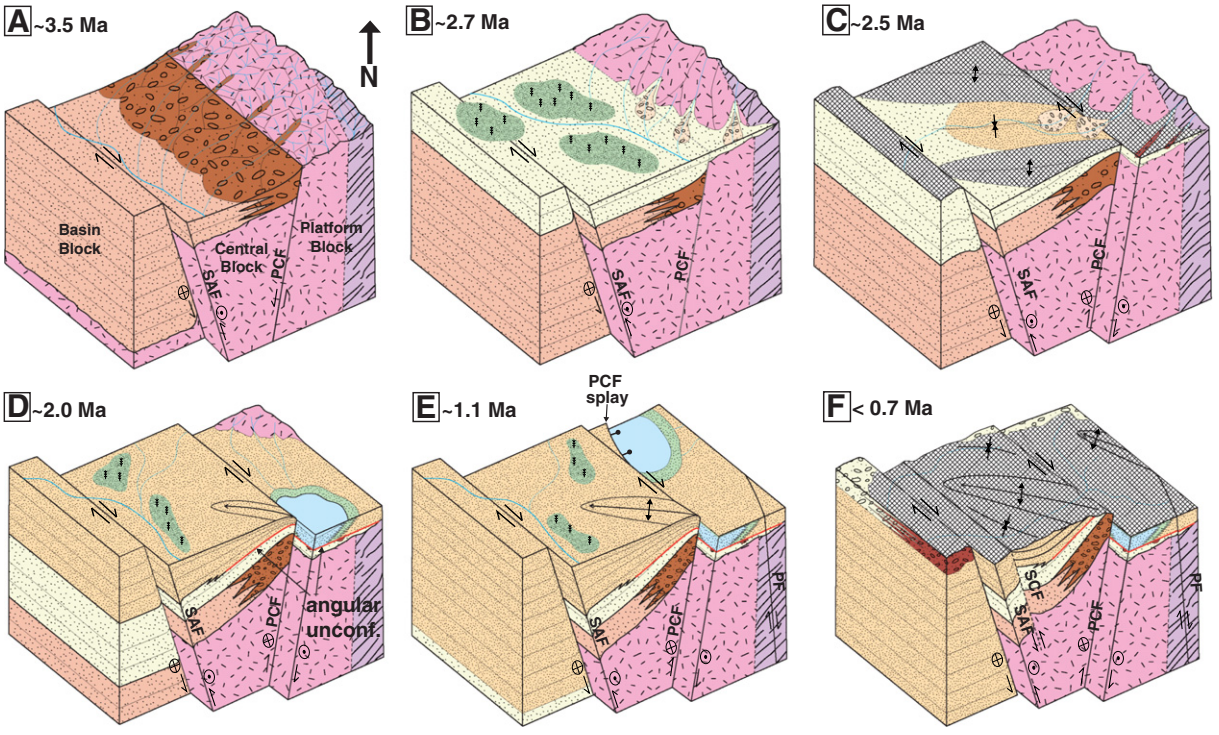

Fig. 16. Block diagrams illustrating the evolution of vertical crustal motions and depositional systems from ~3.5 Ma to the present in the Mecca Hills. (A) SW-side down slip on the PCF and deposition of the Mecca Conglomerate. (B) Overlapping deposition of the regionally extensive facies of the lower member of the Palm Spring Formation on the vertically quiescent PCF. Local conglomerates sourced from nearby basement highlands. (C) SW-side up slip on the PCF created the time-transgressive angular unconformity between the lower and upper members of the Palm Spring Formation, with lateral interfingering of lower and upper Palm Spring Formation locally. (D) Continued SW-side up slip along the PCF is overwhelmed by regional subsidence and sediment accumulation. A lake forms NE of the PCF from pooling water against a topographic high. (E) Initiation of PCF horse-tail splay fault shift the lacustrine depocenter ~4.5 km to the NE. (F) Progradation of Ocotillo Conglomerate and initiation of the modern phase of uplift and transpressional deformation after ca. 0.7 Ma. Initiation of the SCF (Skeleton Canyon fault), and PF (Platform fault).

the fault zone at ~2.6 Ma (Figs. 15C, 16C). Southwest of the PCF, lateral interfingering of the lower and upper Palm Spring members, southeastward thickening of the upper member, and time-transgressive architecture of the unconformity suggest that deposition continued locally in this small area during deformation, erosion, and creation of the unconformity (Figs. 12, 16C) throughout the rest of the Mecca Hills and Indio Hills.

The upper Palm Spring member records a change to more localized fault-controlled sedimentation and SW-side up vertical displacement along the PCF, while persistent regional subsidence and sediment accommodation allowed for continued deposition throughout much of the Mecca Hills. The scouring, localized valley-fill red conglomerates and cobble-lag deposit at the base of the upper Palm Spring member northeast of the PCF (Figs. 6A, 15C, 16C) may record sediment bypass during formation of the unconformity. Above the unconformity near Eagle Canyon, shallow lacustrine deposits of the upper Palm Spring member form a prominent hill adjacent to the PCF (Fig. 8A). We infer that water sourced from local rivers in the Cottonwood Mountains pooled on the northeast side of a topographic high along the PCF (Figs. 15D, 16D). Evidence of this paleotopography includes the presence of recycled lower Palm Spring member sandstone clasts in the upper member (Fig. 7D) and growth strata within the upper member (Fig. 8F) on the northeast side and adjacent to the PCF. SE-directed alluvial fans sourced from the Cottonwood Mountains interacted at their distal ends with this perched-basin lake northeast of the PCF. At ca. 1.0 Ma, the lacustrine depocenter migrated ~4.5 km northwest in response to localized subsidence northeast of a transtensional splay of the PCF (Figs. 15E, 16E). The lake remained fixed at this location until it was filled by prograding Ocotillo Conglomerate derived from the Cottonwood Mountains beginning ~760 ka.

Southwest of the PCF, deposition of the upper Palm Spring member persisted intermittently through deformation that created the two angular unconformities (Figs. 12, 15C, 16C). After formation of the upper unconformity at ~2.3 Ma, it is unclear whether deposition took place on the flank of growing topography, or passively buried a submerged area of uplift SW of the PCF (Figs. 15D, 16D).

Significant slowing of subsidence shortly before 760 ka resulted in rapid basinward progradation of large alluvial fans from the Cottonwood and Orocopia mountains, resulting in deposition of the Ocotillo Conglomerate across most or all of the Mecca Hills (Figs. 15F, 16F). Northeast of the PCF, the Bishop Ash is interbedded in the lower part of the Ocotillo Conglomerate (Figs. 4, 6A), while southwest of the PCF the Bishop and Thermal Canyon ash are interbedded in the uppermost upper Palm Spring member, beneath the Ocotillo gravel (Fig. 4). This relationship implies that progradation of Ocotillo gravel took place at about 760 ka, and supports geomorphic evidence that the gravel was derived from the Cottonwood and Orocopia mountains northeast of the Mecca Hills (Figs. 2, 15F). Thickening of Ocotillo Conglomerate in a localized wedge adjacent to the PCF in upper Painted Canyon records continued subsidence northeast of the PCF splay during Ocotillo progradation (Figs. 15F, 16F). Waning regional subsidence likely caused Ocotillo gravels to prograde during the transition from subsidence and sediment accumulation to the modern phase of uplift and erosion in the Mecca Hills.

5.2. Regional significance of fault-zone evolution

It is well documented that local transpression and transtension within strike-slip fault zones results in significant, rapid, short-lived vertical displacements (e.g. Christie-Blick and Biddle, 1985; Teyssier et al., 1995; Aksu, 2000; Wakabayashi et al., 2004; Mann, 2007). Sinuous and irregular strike-slip fault zones produce localized migrating zones of transpressive and transtensive deformation due to the kinematics of translating rock along non-linear fault surfaces (e.g. Christie-Blick and Biddle, 1985; Spotila et al., 1998; Wakabayashi et al., 2004; Cormier et al., 2006; Benowitz et al., 2011). This can produce rapid local accumulations of sediments that are subsequently uplifted and eroded as they are translated through a complex heterogeneous strain field (e.g., Crowell, 1974; Sadler et al., 1993; Crowell, 2003). Therefore, we expect the spatial and temporal extent of deposits produced by deformation in strike-slip fault zones to be governed by the spatial scale of local fault zone complexities and rates of fault slip.

In the Mecca Hills, the evolution of local structures and the resulting complexly evolving strain field can explain the abundant nonlinear faults, complex history of fault-controlled deposition, reactivation and inversion of the PCF, migration of depocenters, and time-transgressive angular unconformity. This explanation does not require any changes in relative plate motion or regional fault kinematics. According to this conceptual model, all deformation recorded in the stratigraphy of the Mecca Hills is expected to occur at a spatial scale similar to that of local faults and fault-bounded blocks. Similarly, any stratigraphic signals produced by regional-scale tectonic changes should be expressed at a spatial scale significantly larger than that of local fault-zone complexities.

Although many of the sedimentation and deformation patterns in the Mecca Hills clearly record the evolution of local fault-zone complexities, two prominent stratigraphic signals are recognized over a much broader area of the Coachella Valley and therefore must record regional tectonic events. First, the angular unconformity separating the lower and upper members of the Palm Spring Formation is present along ~50 km of the SAF from the SE Mecca Hills to the Indio Hills (Boley, 1993; Boley et al., 1994). The time-transgressive unconformity bracketing syn-kinematic deposits in the central Mecca Hills suggests that widespread deformation and erosion included areas of local subsidence and deposition that buried actively growing structures. This style resembles the modern phase of deformation in which a narrow belt of variable uplift along the Coachella Valley segment of the SAF competes with rapid sediment input, resulting in areas of net uplift and erosion and areas of net burial (e.g. Keller et al., 1982). The age of the unconformity is not well dated in the Indio Hills, so the correlation inferred here has yet to be fully tested. However, the striking regional correlation of this unconformity which separates two regionally correlative members of the Palm Spring Formation suggests that it records a major regional change in fault-zone evolution at ca. 2.6–2.4 Ma.

The second event is recorded in deposits up to and including the Bishop Ash (760 ka) and Thermal Canyon ash (740 ka), which are currently experiencing uplift in a ~90-km long by 2- to 7-km wide belt from Durmid Hill in the southeast to the northern Indio Hills in the northeast (Fig. 1). Prior to 740 ka, variable localized deformation along the SAF in Coachella Valley was superimposed on overall regional subsidence and sediment aggradation. It appears that a major change resembling the ca. 2.6-Ma event has inverted a narrow belt along the fault zone from net subsidence to net uplift and erosion that started shortly after 740 ka. This tectonic event may be recorded in other areas of the southern SAF system, as seen in the onset of contractional deformation in the southern San Jacinto fault zone at ~0.6 Ma (Steely et al., 2009; Lutz et al., 2006; Kirby et al., 2007), and the onset of rapid uplift and exhumation of fault-bounded crustal slices along the SAF in San Gorgonio Pass at ~0.7 Ma (Spotila et al., 1998).

Changes in regional kinematics of the southern SAF zone may be linked to major reorganizations of the plate boundary system through time. Changes in regional fault-zone deformation could be related to variations in partitioning of slip rates between the San Jacinto fault and SAF through time (e.g., Bennett et al., 2004), or between the SAF through San Gorgonio Pass and transfer of strain northward through the Eastern Transverse Ranges into the Eastern California Shear zone (e.g., Dolan et al., 2007). In these models, differential alternating slip along crustal-scale faults results in block rotations and deformation at their margins (e.g. Nilsen and Sylvester, 1995). A major reorganization occurred at ~1.3–1.1 Ma when a significant fraction of plate-boundary motion was transferred from the southern SAF to the newly formed San Jacinto fault (e.g., Janecke et al., 2010). Other than initiation or

acceleration of slip along the PCF splay, however, there is no evidence for major deformation in the Mecca Hills at this time. Thus it appears that the southern the SAF did not experience a major structural reorganization when slip was transferred to the emerging San Jacinto fault zone.

To the southeast, Aragón-Arreola and Martín-Barajas (2007) presented marine seismic evidence for a westward shift and localization of faults and basins in the northern Gulf of California during a regional tectonic reorganization that is bracketed in time between roughly 3.3 and 2.0 Ma. The area affected by this reconfiguration extends north at least to the south end of the modern Salton Sea, ~50 km SE of the Mecca Hills (Fig. 1; Aragón-Arreola and Martín-Barajas, 2007), and may have included the Coachella Valley. We suggest that regional-scale deformation that created the 2.6- to 2.3-Ma angular unconformity in the Mecca Hills may be kinematically linked to the tectonic reorganization in the northern Gulf of California. If correct, this would suggest a refined age of about 2.6–2.3 Ma for the offshore tectonic event, or perhaps somewhat older if it propagated from SE to NW. The effects of this event in the Coachella Valley remain incompletely understood and represent a topic for future study.

6. Conclusions

Our stratigraphic analysis reveals a 3–5 Myr history of complex basin development and deformation along the Mecca Hills segment of the southern SAF. The tectonostratigraphic framework in this area records a paleo-landscape that changed dramatically in response to rapid, punctuated, alternating periods of subsidence and uplift. Several regionally correlative tectonic events in the Mecca Hills are overprinted by smaller-scale patterns of deposition that are likely related to the evolution of local geometric complexities in the fault zone.

Deformation associated with slip along the PCF largely controlled the distribution of deposition in the central Mecca Hills. Beginning ~3.7 Ma, SW-side down slip on the PCF resulted in deposition of the Mecca Conglomerate on the central block in SW-directed alluvial fans sourced from the platform block to the northeast. From ~3.0–2.6 Ma, vertical quiescence along the PCF and regional subsidence lead to deposition of the lower member of the Palm Spring Formation throughout the Mecca Hills in a large SE-directed fluvial system that occupied the paleo-Coachella Valley.

At ~2.6 Ma, initiation of SW-side up slip along the PCF and associated near-field transpressional deformation uplifted, eroded and folded deposits of the central block, partitioning deposition northeast and southwest of the PCF and creating a major angular unconformity between the lower and upper members of the Palm Spring Formation. The unconformity is observed along ~50 km of the Coachella Valley segment of the SAF and varies from highly angular to nearly conformable and time-transgressive, recording spatially variable, synchronous uplift and burial similar to modern deformation along the southern SAF. Post 740-ka renewed or accelerated SW-side up slip on the PCF and other structures along the Coachella Valley segment of the SAF lead to the modern phase of uplift, transpression and erosion.

Two regionally correlative changes in deformation along the Coachella Valley segment of the SAF probably have been controlled by plate boundary-scale changes in partitioning of slip through time. We propose that the 2.6–2.3 Ma angular unconformity in the Mecca Hills records a short-live pulse of regional-scale deformation that may be linked to a well-documented but poorly dated tectonic reorganization in the northern Gulf of California (Aragón-Arreola and Martín-Barajas, 2007). A second regional change at ca. 740 ka – from regional subsidence and sedimentation to regional uplift and erosion along the entire Coachella Valley segment of the southern SAF – remains poorly understood.

Supplementary data to this article can be found online at http://dx.doi.org/10.1016/j.tecto.2017.03.021.

Acknowledgments

This work was funded by National Science Foundation grants EAR-1144946 to Rebecca Dorsey and EAR-1144355 to Bernard Housen. Ray Ingersoll and an anonymous reviewer provided valuable input that improved the final version of the paper. We thank Ray Weldon for helpful insights and discussions during the course of the research.

References

Aksu, A.E., Calon, T.J., Hiscott, R.N., Yasar, D., 2000. Anatomy of the North Anatolian Fault Zone in the Marmara Sea, Western Turkey: extensional basins above a continental transform. Geological Society of America Today vol. 10, 3–7.

Aragón-Arreola, M., Martín-Barajas, A., 2007. Westward migration of extension in the northern Gulf of California, Mexico. Geology vol. 35:571–574. http://dx.doi.org/10.1130/G23360A.1.

Atwater, T., 1970. Implications of plate tectonics on the Cenozoic tectonic evolution of Western North America. Geol. Soc. Am. Bull. vol. 81, 3513–3536.

Axen, G.J., Fletcher, J.M., 1998. Late Miocene-Pleistocene extensional faulting, northern Gulf of California, Mexico and Salton Trough, California. Int. Geol. Rev. vol. 40, 217–244.

Behr, W.M., Rood, D.H., Fletcher, K.E., Guzman, N.E., Finkel, R., Hanks, T.C., Hudnut, K.W., Kendrick, K.J., Platt, J.P., Sharp, W.D., Weldon, R.J., Yule, J.D., 2010. Uncertainties in slip rate estimates for the Mission Creek strand of the southern San Andreas fault at Biskra Palms oasis: southern California. Geol. Soc. Am. Bull. vol. 122, 1360–1377.

Bennett, R.A., Friedrich, A.M., Furlong, K.P., 2004. Codependent histories of the San Andreas and San Jacinto fault zones from inversion of fault displacement rates. Geology vol. 32, 961–964.

Benowitz, J.A., Layer, P.W., Armstrong, P., Perry, S.E., Haeussler, P.J., Fitzgerald, P.G., Van Laningham, S., 2011. Spatial variations in focused exhumation along a continental-scale strike-slip fault: the Denali fault of the eastern Alaska Range. Geosphere vol. 7, 455–467.

Blair, T.C., 1987a. Sedimentary processes, vertical stratification sequences, and geomorphology of the Roaring River alluvial fan, Rocky Mountain National Park, Colorado. J. Sediment. Petrol. vol. 57, 1–18.

Blair, T.C., McPherson, J.G., 1994. Alluvial fans and their natural distinction from rivers based on morphology, hydraulic processes, sedimentary processes, and facies assemblages. J. Sediment. Res. vol. 64, 450–489.

Boley, J.L., 1993. Block Rotation and Magnetostratigraphy Along the Southern San Andreas Fault Zone, California. [MS. thesis]. University of Oregon (200 pp).

Boley, J.L., Stimac, J.P., Weldon, R.J., Rymer, M.J., 1994. Stratigraphy and paleomagnetism of the Mecca and Indio Hills, southern California. In: McGill, S.F., Ross, T.M. (Eds.), Geological Investigations of an Active Margin: Geological Society of America. Cordilleran Section Guidebook, Trip 15, pp. 336–344.

Chang, S.-B.R., Allen, C.R., Kirschvink, J.L., 1987. Magnetic stratigraphy and a test for block rotation of sedimentary rocks within the San Andreas fault zone, Mecca Hills, southeastern California. Quat. Res. vol. 27, 30–40.

Christie-Blick, N., Biddle, K.T., 1985. Deformation and basin formation along strike-slip faults. In: Biddle, K.T., Christie-Blick, N. (Eds.), Strike-Slip Deformation, Basin Formation, and Sedimentation. SEPM Special Publication 37, pp. 1–34.

Cormier, M.H., Seeber, L., McHugh, C.M.G., Polonia, A., Cagatay, M.N., Emre, O., Gasperini, L., Gorur, N., Bertoluzzi, G., Bonatti, E., Ryan, W.B.F., Newman, K.R., 2006. The North Anatolian fault in the Gulf of Izmit (Turkey): rapid vertical motion in response to minor bends of a non-vertical continental transform. J. Geophys. Res. vol. 111, B04102 (doi: 0.1029/2005JB003633).

Crowell, J.C., 1974. Origin of late Cenozoic basins in southern California. In: Dickinson, W.R. (Ed.), Tectonics and Sedimentation. SEPM Special Publication 22, pp. 190–204.

Crowell, J.C., 2003. Evolution of Ridge Basin, Southern California: An Interplay of Sedimentation and Tectonics: Geological Society of America Special Paper. p. 367 (247).

Dibblee Jr., T.W., 1954. Geology of the Imperial Valley region, California. Geology of Southern California, California Division of Mines Bulletin vol. 170, 21–28.

Dibblee, T.W., 1997. Geology of the southeastern San Andreas fault zone in the Coachella Valley area, southern California. In: Baldwin, et al. (Eds.), Southern San Andreas Fault – Whitewater to Bombay Beach, Salton Trough, California. South Coast Geological Society (Field Trip Guidebook No. 25, p. 35–56).

Dimitroff, Cassidy W., 2015. Paleomagnetic Determination of Vertical-Axis Block Rotation and Magnetostratigraphy in the Mecca Hills and Coachella Valley, California. [MS Thesis]. Western Washington University (73 pp).

Dolan, J.F., Bowman, D.D., Sammis, C.G., 2007. Long-range and long-term fault interactions in southern California. Geology vol. 35 (9):855–858. http://dx.doi.org/10.1130/G23789A.1.

Dorsey, R.J., 2010. Sedimentation and crustal recycling along an active oblique-rift margin: Salton Trough and northern Gulf of California. Geology vol. 38, 443–446.

Dorsey, R.J., Axen, G.J., Peryam, T.C., Kairouz, M.E., 2012. Initiation of the southern Elsinore fault at ~1.2 Ma: evidence from the Fish Creek–Vallecito Basin, southern California. Tectonics vol. 31:TC2006. http://dx.doi.org/10.1029/2011TC003009.

Dorsey, R.J., Housen, B.A., Janecke, S.U., Fanning, C.M., Spears, A.L.F., 2011. Stratigraphic record of basin development within the San Andreas fault system: Late Cenozoic Fish Creek-Vallecito basin, southern California. Geol. Soc. Am. Bull. vol. 123, 771–793.

Dorsey, R.J., Langenheim, V.E., 2015. Crustal-scale tilting of the central Salton block, southern California. Geosphere vol. 11 (5) 19 pages. 10.1130/GES01167.1.

Elders, W.A., Sass, J.H., 1988. The Salton Sea scientific drilling project. J. Geophys. Res. 93 (Issue B11), 12,953–12,968.

Elmore, R.D., Dulin, S., Engel, M.H., Parnell, J., 2006. Remagnetization and fluid flow in the Old Red Sandstone along the Great Glen Fault, Scotland. J. Geochem. Explor. vol. 89, 96–99.

Fattaruso, L., Cooke, M.L., Dorsey, R.J., 2014. Sensitivity of uplift patterns to dip of the San Andreas fault in the Coachella Valley, CA. Geosphere vol. 10, 1235–1246.
Fattaruso, L.A., Cooke, M.L., Dorsey, R.J., Housen, B.A., 2016. Response of deformation patterns to reorganization of the southern San Andreas fault system since ca. 1.5 Ma. Tectonophysics 693, 474–488.
Fuis, G.S., Scheirer, D.S., Langenheim, V.E., Kohler, M.D., 2012. A new perspective on the geometry of the San Andreas fault in southern California and its relationship to lithospheric structure. Bull. Seismol. Soc. Am. 102:236–251. http://dx.doi.org/10.1785/0120110041.
Fuis, G.S., Mooney, W.D., Healy, J.H., McMechan, G.A., Lutter, W.J., 1984. A seismic refraction survey of the Imperial Valley Region, California. J. Geophys. Res. vol. 89, 1165–1189.
Gordon, I., Heller, P.L., 1993. Evaluating major controls on basinal stratigraphy, Pine Valley, Nevada: implications for syntectonic deposition. Geol. Soc. Am. Bull. vol. 105 (1), 47–55.
Gray, H.J., Owen, L.A., Dietsch, C., Beck, R.A., Caffee, M.A., Finkel, R.C., Mahan, S.A., 2014. Quaternary landscape development, alluvial fan chronology and erosion of the Mecca Hills at the southern end of the San Andreas Fault zone. Quat. Sci. Rev. vol. 105, 66–85.
Hampton, B.A., Horton, B.K., 2007. Sheetflow fluvial processes in a rapidly subsiding basin, Altiplano plateau, Bolivia. Sedimentology vol. 54, 1121–1147.
Heller, P.L., Paola, C., 1992. The large-scale dynamics of grain-size variations in alluvial basins 2. Application to syntectonic conglomerate. Basin Res. vol. 4, 91–102.
Housen, B.A., van der Pluijm, B.A., Van der Voo, R., 1993. Magnetite dissolution and neocrystallization during cleavage formation: paleomagnetic study of the Martinsburg Formation, Lehigh Gap, Pennsylvania. J. Geophys. Res. vol. 98, 13,799–13,813.
Ingersoll, R.V., Pratt, M.J., Davis, P.M., Caracciolo, L., Day, P.P., Hayne, P.O., Petrizzo, D.A., Gingrich, D.A., Cavazza, W., Critelli, S., Diamond, D.S., Coffey, K.T., Stang, D.M., Hoyt, J.F., Reith, R.C., Hendrix, E.D., 2014. Paleotectonics of a complex Miocene half graben formed above a detachment fault: the Diligencia basin, Orocopia Mountains, southern California. Lithosphere vol. 6:157–176. http://dx.doi.org/10.1130/L334.1.
Ingersoll, R.V., Rumelhart, P.E., 1999. Three-stage evolution of the Los Angeles Basin, southern California. Geology 27, 593–596.
Jacobson, C.E., Grove, M., Vucic, A., Pedrick, J.N., Ebert, K.A., 2007. Exhumation of the Orocopia Schist and associated rocks of southeastern California: relative rates of erosion, synsubduction tectonic denudation, and middle Cenozoic extension. In: Cloos, M., et al. (Eds.), Convergent Margin Terranes and Associated Regions: A Tribute to W.G. Ernst. Geological Society of America Special Paper 419, pp. 1–37.
Janecke, S.U., Dorsey, R.J., Steely, A.N., Kirby, S.M., Lutz, A.T., Housen, B.A., Belgarde, B., Langenheim, V., Rittenour, T., Forand, D., 2010. High geologic slip rates since early Pleistocene initiation of the San Jacinto and San Felipe fault zones in the San Andreas fault system: southern California, USA. Geol. Soc. Am. Spec. Pap. vol. 48, 475.
Katz, B., Elmore, R.D., Cogoini, M., Ferry, S., 1998. Widespread chemical remagnetization: orogenic fluids or burial diagenesis of clays? Geology vol. 26, 603–606.
Keller, E.A., Bonkowski, M.S., Korsch, R.J., Shlemon, R.J., 1982. Tectonic geomorphology of the San Andreas fault zone in the Southern Indio Hills, Coachella Valley, California. Geol. Soc. Am. Bull. vol. 93, 46–56.
Kirby, S.M., Janecke, S.U., Dorsey, R.J., Housen, B.A., Langenheim, V., McDougall, K., Steely, A.N., 2007. Pleistocene Brawley and Ocotillo formations: evidence for initial strike-slip deformation along the San Felipe and San Jacinto fault zones, southern California. Geology vol. 115:43–62. http://dx.doi.org/10.1086/509248.
Langenheim, V.E., Jachens, R.C., Matti, J.C., Hauksson, E., Christensen, A., 2005. Geophysical evidence for wedging in the San Gorgonio Pass structural knot, southern San Andreas fault zone, southern California. Geol. Soc. Am. Bull. vol. 117, 1554–1572.
Law, R.D., Eriksson, Kenneth, Davisson, Cole, 2001. Formation, evolution, and inversion of the middle Tertiary Diligencia basin, Orocopia Mountains, southern California. Geol. Soc. Am. Bull. vol. 113, 196–221.
Lekic, V., French, S.W., Fischer, K.M., 2011. Lithospheric thinning between rifted regions 582 of southern California. Science vol. 334, 783–787.
Lin, G., Shearer, P.M., Hauksson, E., 2007. Applying a three-dimensional velocity model, waveform cross-correlation, and cluster analysis to locate southern California seismicity from 1981 to 2005. J. Geophys. Res. 112, B12309 (doi: 10/1029/2007JB004986).
Lindsey, E.O., Fialko, Y., 2013. Geodetic slip rates in the southern San Andreas Fault system: effects of elastic heterogeneity and fault geometry. J. Geophys. Res. Solid Earth 118:689–697. http://dx.doi.org/10.1029/2012JB009358.
Lutz, A.T., Dorsey, R.J., Housen, B.A., Janecke, S.U., 2006. Stratigraphic record of Pleistocene faulting and basin evolution in the Borrego Badlands, San Jacinto fault zone, southern California. Geol. Soc. Am. Bull. vol. 118:1377–1397. http://dx.doi.org/10.1130/B25946.1.
Mann, P., 2007. Global catalogue, classification and tectonic origins of restraining and releasing bends on active and ancient strike-slip fault systems. In: Cunningham, W.D., Mann, P. (Eds.), Tectonics of Strike-Slip Restraining and Releasing Bends. Geological Society of London Special Publication vol. 290, pp. 13–142.
Matti, J.C., Morton, D.M., 1993. Paleogeographic evolution of the San Andreas fault in southern California: a reconstruction based on a new cross-fault correlation. In: Powell, R.E., Weldon II, R.E., Matti, J.C. (Eds.), The San Andreas Fault System: Displacement, Palinspastic Reconstruction, and Geologic Evolution. Geological Society of America Memoir 178, pp. 107–159.
McNabb, J.C., 2013. Stratigraphic Record of Pliocene-Pleistocene Basin Evolution Along the Southern San Andreas Fault, Mecca Hills California. [MS Thesis]. University of Oregon (58 pp).
Messé, Graham T., 2014. Magnetostratigraphy and Block Rotation of the Mecca Hills, CA. [MS Thesis]. Western Washington University (57 pp).
Miall, A.D., 1985. Architectural element analysis: a new method of facies analysis applied to fluvial deposits. Earth Sci. Rev. vol. 22, 261–308.
Miller, D.D., 1998. Distributed shear, rotation, and partitioned strain along the San Andreas fault, central California. Geology vol. 26, 867–870.
Morton, D.M., Matti, J.C., 1993. Extension and contraction within an evolving divergent strike-slip fault complex: the San Andreas and San Jacinto fault zones at their convergence in southern California. In: Powell, R.E., Weldon, R.J., Matti, J.C. (Eds.), The San Andreas Fault System: Displacement, Palinspastic Reconstruction, and Geologic Evolution. Geological Society of America, Memoir vol. 178, pp. 217–230.
Mulder, T., Alexander, J., 2001. The physical character of subaqueous sedimentary density flows and their deposits. Sedimentology vol. 48, 269–299.
Nichols, G.J., Hirst, J.P.P., 1998. Alluvial fans and fluvial distributary systems, Oligo-Miocene, northern Spain: contrasting processes and products. J. Sediment. Res. vol. 68, 879–889.
Nilsen, T.H., Sylvester, A.G., 1995. Strike-Slip Basins. Tectonics of Sedimentary Basins. pp. 425–457.
Oskin, M., Stock, J., 2003a. Marine incursion synchronous with plate boundary localization in the Gulf of California. Geology vol. 31:23–26. http://dx.doi.org/10.1130/00917613(2003)031<0023:MISWPB>2.0.CO;2.
Oskin, M., Stock, J., 2003b. Pacific–North America plate motion and opening of the Upper Delfín basin, northern Gulf of California, Mexico. Geol. Soc. Am. Bull. vol. 115: 1173–1190. http://dx.doi.org/10.1130/B25154.1.
Paola, C., Heller, P.L., Angevine, C.L., 1992. The large scale dynamics of grain-size variations in alluvial basins, 1. Theory. Basin Res. vol. 4, 73–90.
Parsons, T., McCarthy, J., 1996. Crustal and upper mantle velocity structure of the Salton Trough, southeast California. Tectonics vol. 15, 456–471.
Rymer, M.J., 1991. Geologic structure, transpression, and neotectonics of the San Andreas Fault in the Salton Trough, California; Part 2, The Bishop ash bed in the Mecca Hills. In: Geological excursions in southern California and Mexico. Geological Society of America Annual Meeting Guidebook: San Diego State Univ, San Diego, CA, pp. 388–396.
Rymer, M.J., 1994. Quaternary fault-normal thrusting in the northwestern Mecca Hills, southern California. In: McGill, S.F., Ross, T.M (Eds.), Geological investigations of an active margin: Guidebook, 1994. Cordilleran Section, Geological Society of America, pp. 325–329.
Sadler, P., Demirer, A., West, D., Hillenbrand, J.M., 1993. The Mill Creek Basin, the Potato Sandstone, and fault strands in the San Andreas fault zone south of the San Bernardino Mountains. In: Powell, R.E., Weldon, R.J., Matti, J.C. (Eds.), The San Andreas Fault System: Displacement, Palinspastic Reconstruction, and Geologic Evolution. Geological Society of America Memoir vol. 178, pp. 289–306.
Seeber, L., Cormier, M.-H., McHugh, C., Emre, Ö., Polonia, A., Sorlien, C., 2006. Rapid subsidence and sedimentation from oblique slip near a bend on the North Anatolian Transform in the Marmara Sea, Turkey. Geology vol. 34, 933–936.
Seeber, L., Sorlien, C., Steckler, M., Cormier, M.H., 2010. Continental transform basins: why are they asymmetric? Eos vol. 91 (4), 29–30.
Sheridan, J.M., Weldon II, R.J., 1994. Accommodation of compression in the Mecca Hills, California. In: McGill, S.F., Ross, T.M. (Eds.), Geological Investigations of an Active Margin: Guidebook, 1994, Geological Society of America, Cordilleran Section. San Bernardino County Museum, Redlands, California, pp. 330–336.
Sieh, K.E., Williams, P.L., 1990. Behavior of the southernmost San Andreas fault during the past 330 years. J. Geophys. Res. vol. 95, 6629–6645.
Spotila, J.A., Farley, K.A., Sieh, K., 1998. Uplift and erosion of the San Bernardino Mountains, associated with transpression along the San Andreas fault, CA, as constrained by radiogenic helium thermochronometry. Tectonics vol. 17, 360–378.
Spotila, J.A., House, M.A., Niemi, N.A., Brady, R.C., Oskin, M., Buscher, J.T., 2007a. Patterns of bedrock uplift along the San Andreas fault and implications for mechanisms of transpression. In: Till, A.B., Roeske, S.M., Sample, J.C., Foster, D.A. (Eds.), Exhumation Associated With Continental Strike-Slip Fault Systems. Geological Society of America Special Paper 434, pp. 15–33.
Spotila, J.A., Niemi, N.A., Brady, R.C., House, M.A., Buscher, J.T., Oskin, M., 2007b. Longterm continental deformation associated with transpressive plate motion: the San Andreas fault. Geology vol. 35, 967–970.
Steely, A.N., Janecke, S.U., Dorsey, R.J., Axen, G.J., 2009. Early Pleistocene initiation of the San Felipe fault zone, SW Salton Trough, during reorganization of the San Andreas fault system. Geol. Soc. Am. Bull. vol. 121, 663–687.
Stock, J.M., Hodges, K.V., 1989. Pre-Pliocene extension around the Gulf of California and the transfer of Baja California to the Pacific Plate. Tectonics vol. 8:99–115. http://dx.doi.org/10.1029/TC008i001p00099.
Sylvester, A.G., 1999. Rifting, transpression, and neotectonics in the central Mecca Hills, Salton Trough. In: Cooper, J.D. (Ed.), Pacific Section SEPM Fall Field Trip Guidebook. Pacific Section SEPM Book 85, pp. 1–11.
Sylvester, A.G., Smith, R.R., 1976. Tectonic transpression and basement-controlled deformation in San Andreas fault zone, Salton Trough, California. Am. Assoc. Pet. Geol. Bull. vol. 60, 2081–2102.
Teyssier, C., Tikoff, B., Markley, M., 1995. Oblique plate motion and continental tectonics. Geology vol. 23, 447–450.
Wakabayashi, J., Hengesh, J.V., Sawyer, T.L., 2004. Four-dimensional transform fault processes: progressive evolution of stepovers and bends. Tectonophysics vol. 392 (1–4), 279–301.
Weldon, R.J., Meisling, K.E., Alexander, J., 1993. A speculative history of the San Andreas fault in the Transverse Ranges, California. In: Powell, R.E., Weldon, R.J., Matti, J.C. (Eds.), The San Andreas Fault System: Displacement, Palinspastic Reconstruction, and Geologic Evolution. Geological Society of America Memoir vol. 178, pp. 161–198.
Wilcox, R.E., Harding, T.P., Seely, R., 1973. Basic wrench tectonics. Am. Assoc. Pet. Geol. Bull. vol. 57, 74–96.
Yule, D., Sieh, K., 2003. Complexities of the San Andreas fault near San Gorgonio Pass: implications for large earthquakes. J. Geophys. Res. vol. 108 (B11) (ETG 9-1–9-23, doi: 10.1029/2001JB000451).